Available online at www.sciencedirect.com
SCIENCE DIRECT®
Journal of Sound and Vibration 290 (2006) 1202–1233
JOURNAL OF SOUND AND VIBRATION
www.elsevier.com/locate/jsvi

"Buzz-saw" noise: A comparison of measurement with prediction

A. McAlpine[a,*], M.J. Fisher[a], B.J. Tester[b,1]

[a]*Institute of Sound and Vibration Research, University of Southampton, Southampton SO17 1BJ, England, UK*
[b]*Rolls–Royce plc, Derby, P.O. Box 31, DE24 8BJ, England, UK*

Received 29 June 2004; received in revised form 22 March 2005; accepted 16 May 2005
Available online 18 August 2005

Abstract

Accurate prediction of "buzz-saw" noise in a turbofan inlet duct necessitates consideration of nonlinear acoustics, modelling a complete fan blade set, modelling an acoustic liner, and calculations at high frequencies. A recent series of papers has described new work concerning the application of one-dimensional propagation models to the prediction of buzz-saw noise. A numerical model, termed the frequency domain numerical solution or FDNS, has been developed. It can be used to calculate the nonlinear propagation of the rotor-alone pressure field in either a rigid or acoustically-lined inlet duct. From this the in-duct noise level of the buzz-saw tones can be determined. In previous work, validation of this method by comparison with in-duct noise measurements has been limited to rigid inlet ducts, because of the lack of availability of suitable measurements from lined ducts. In this article new measurements of buzz-saw noise in an acoustically-lined inlet duct are utilized. A comparison of measurements of buzz-saw noise in a lined inlet duct, and noise predictions from numerical simulations by the FDNS is presented. The detailed measurements reveal the effect of an acoustic liner on buzz-saw noise. The suitability of the numerical model to be used to provide realistic noise predictions for supersonic ducted fans is also examined.

*Corresponding author. Tel.: +44 23 8059 2291; fax: +44 23 8059 3190.
E-mail address: am@isvr.soton.ac.uk (A. McAlpine).
[1]Present address: Institute of Sound and Vibration Research, University of Southampton, Southampton SO17 1BJ, England, UK.

0022-460X/$ - see front matter © 2005 Elsevier Ltd. All rights reserved.
doi:10.1016/j.jsv.2005.05.028

1. Introduction

"Buzz-saw" noise is associated with the type of modern high-bypass-ratio turbofan aircraft engine that first entered service in the 1970s. The use of higher bypass ratios led to turbofan engines with larger fans. These engines operate, notably during take-off and climb, with fan tip speeds that exceed sonic velocity. At supersonic fan speeds, an acoustic signature is radiated forward of the fan containing tones at harmonics of the engine's shaft rotation frequency $\mathscr{F}$. These harmonics are known as the engine orders (EO); the mth harmonic is $\mathrm{EO} = m\mathscr{F}/\mathscr{F} = m$. Buzz-saw noise is the spectrum of EO tones generated by a supersonic ducted fan.[2] The term "buzz-saw" was introduced because originally this noise source was identified by its low pitch and ragged quality, compared with the higher pitched whine associated with earlier generations of turbofan engine. This is because the buzz-saw noise source is typically due to the low-order EO tones, at frequencies less than blade passing frequency (BPF), that dominate the noise frequency spectrum. Buzz-saw noise affects both cabin and community noise levels, and with the design of new and larger aircraft engines, it is likely to remain a prevalent noise source from modern turbofan engines.

It is helpful to consider fan tones in terms of acoustic modes in a duct. A turbofan inlet duct can be modelled approximately by a circular-section cylindrical duct. Then fan tones can be expressed in terms of spinning modes of a cylindrical duct, with azimuthal and radial order m and n, respectively.

The principal source of buzz-saw noise is the "rotor-alone" pressure field. This is the steady, in the rotor's frame of reference, pressure field locked to the rotor. At subsonic fan speeds, the rotor-alone pressure field is cut-off. At supersonic fan speeds, the rotor-alone pressure field propagates upstream in the inlet duct against the oncoming flow. So, buzz-saw noise typically occurs at high engine power operating conditions.

In terms of modes, the rotor-alone pressure field is comprised of spinning modes that have the same circumferential phase velocity as the fan, that is angular frequency ω divided by m equals $2\pi\mathscr{F}$. The frequencies of these modes are multiples of $\mathscr{F}$, i.e. EO tones. Therefore, the rotor-alone pressure field can be expressed in terms of steady modes that are identifiable because they have azimuthal order $m = \mathrm{EO}$.

There are other sources of buzz-saw noise. For example, EO tones can also be generated by the interaction of the rotor-alone pressure field with inlet flow distortions (circumferential variations in the mean flow). In terms of modes this generates, in the rotor's frame of reference, unsteady modes with azimuthal order $m \neq \mathrm{EO}$.

However, buzz-saw noise is principally caused by the generation *and* nonlinear propagation of the rotor-alone pressure field in a turbofan inlet duct. The underlying mechanisms controlling buzz-saw noise have been reasonably well understood since the 1970s, for example see Refs. [1–6]. A detailed description of the formation of buzz-saw noise is in Ref. [7], so only a brief outline is included in this article.

At supersonic fan speeds, the rotor-alone pressure field is comprised of a series of shock- and expansion-waves that extend upstream of the fan. Each shock is located at, or close to, the leading edge of a fan blade. The steady field is shown sketched in Fig. 1. In a direction normal to the

[2]"Buzz-saw" tones are also known as "multiple pure" and "combination" tones.

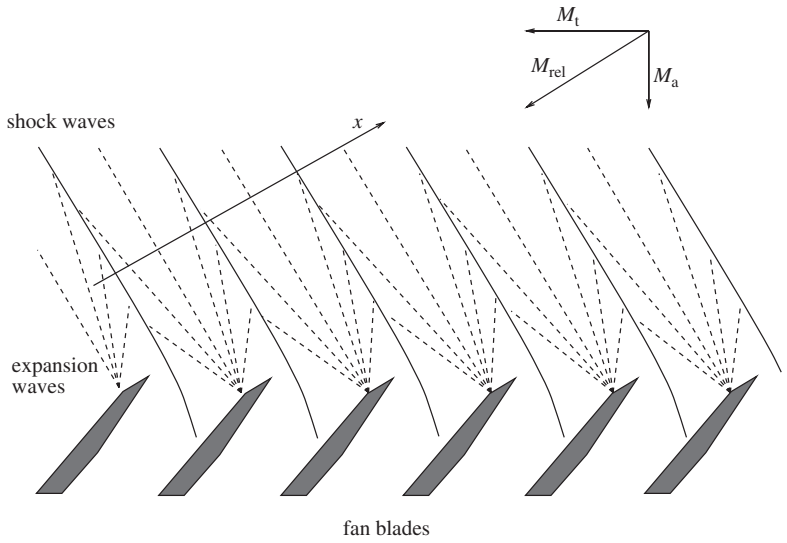

Fig. 1. Shock-wave generation by a supersonic fan. M_a and M_t are the Mach numbers of the inlet flow and fan rotor blade tips, respectively. In the rotor's frame of reference there is a steady flow with Mach number $M_{\text{rel}} = \sqrt{M_a^2 + M_t^2}$ impinging on the leading edge of each fan blade. (After McAlpine and Fisher [7, Fig. 1].)

shocks, denoted by x, the pressure waveform resembles a sawtooth (or N-wave). If the sawtooth is regular,[3] and the shocks can be assumed to be "weak", then all the shocks propagate upstream of the fan at the undisturbed speed of sound, relative to the oncoming fluid. The pressure signature remains a regular sawtooth, with shock strength that decays asymptotically as z^{-1}, where z is the axial distance upstream of the fan. This nonlinear attenuation of a regular sawtooth is explained in Ref. [8].

However, in practice there will be small blade-to-blade variations in the sawtooth waveform, caused largely by variations in the blades' stagger angles, see Ref. [6]. In this case, the velocity of each shock is dependent on its mid-point pressure (weak-shock theory, for example see Ref. [7], Eq. (4)). Therefore, in an irregular sawtooth waveform, the shocks propagate at slightly different speeds relative to each other. As the sawtooth propagates, following a helical path inside the inlet duct, the blade-to-blade periodicity in the waveform becomes less.

The frequency spectrum of an irregular sawtooth waveform will contain tones at each EO harmonic. This is known as the EO frequency spectrum. Close to the fan, the EO frequency spectrum will be dominated by tones at EO $= B, 2B, 3B$, etc, (B is the number of fan blades). These tones are the BPF harmonics. It is the nonlinear propagation of the high-amplitude sawtooth waveform, which leads to the redistribution of energy amongst the EOs, (as the sawtooth becomes more irregular). The amplitude of each EO tone can be modified by nonlinear interactions between the EOs. The principal effect is that energy, initially at harmonics of BPF, is redistributed amongst the other EOs.

[3]This means there are no blade-to-blade variations in the waveform.

Also, energy is dissipated by the shocks. This process is more efficient at high frequencies, so the transfer of energy from low to high frequencies can increase the dissipation. The process of energy being transferred between different EOs, and being dissipated by the shocks, is referred to as "nonlinear attenuation". Most of the nonlinear attenuation occurs close to the fan where the sound pressure level (SPL) is high.

Typically, the nonlinear propagation of the sawtooth waveform leads, by the end of the inlet duct, to the EO frequency spectrum being dominated by tones with $EO < B$. This is a well-known feature of the buzz-saw signature of a supersonic fan. Fig. 2 shows a simple example of the formation of a buzz-saw noise signature. The EO tone levels by the end of the inlet duct have been attenuated as a result of the nonlinear propagation of the waveform. In a rigid inlet duct, it is this nonlinear attenuation which provides the mechanism through which sound energy is dissipated.

In practice, modern turbofan inlet and bypass ducts have acoustic lining on the duct wall. The type of locally-reacting cavity liners that are used in aero-engines tend to have an optimum frequency range. The inclusion of a duct liner is anticipated to highly absorb some of the EO tones, changing the overall nature of the buzz-saw noise spectrum. Not all the EO tones will be well absorbed by the liner. The dimensionless frequency, or Helmholtz number, of the mth BPF harmonic is $kb = mBM_t$, where k is the acoustic wavenumber, b is the radius of the duct and M_t is the rotor blade tip Mach number. Modern fans typically have between 20 and 30 fan blades. Therefore, at BPF the Helmholtz number kb is typically between 20 and 30. Large-amplitude tones

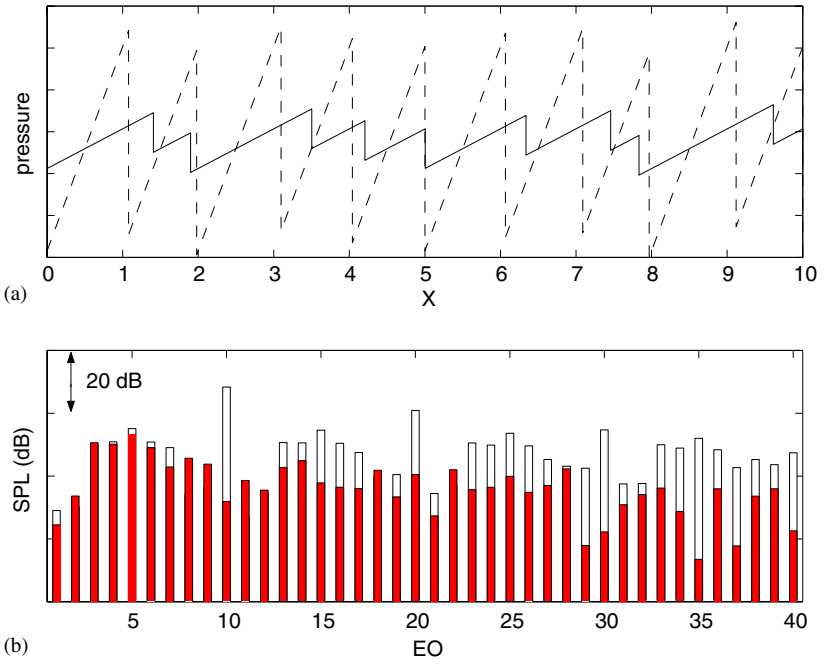

Fig. 2. Example of the formation of a buzz-saw noise signature. (a) - - -, irregular sawtooth pressure waveform close to the fan; —, irregular sawtooth pressure waveform near the end of the inlet duct. (b) EO frequency spectrum close to the fan (white bars); EO frequency spectrum near the end of the inlet duct (grey bars). Note in this example the fan has only 10 rotor blades, i.e. BPF is EO = 10. X is non-dimensional distance in direction x shown in Fig. 1.

tend to be generated at frequencies up to at least 4 BPF, or kb of the order of 100. The optimum frequency range of a cavity liner depends on the fan speed, and is unlikely to extend up to $kb = 100$.

To summarize, accurate prediction of buzz-saw noise in a turbofan inlet duct necessitates the following: nonlinear acoustics because of the high SPLs in an inlet duct; modelling a complete fan blade set to include the irregularity in the sawtooth pressure waveform; modelling an acoustic duct liner; calculations at high frequencies up to kb of the order of 100. Thus, prediction of buzz-saw noise is currently regarded as a challenging problem in computational aeroacoustics.

A recent series of papers by Fisher et al. [7,9,10] has described new work concerning the application of one-dimensional nonlinear propagation models to the prediction of buzz-saw noise. The key step in this recent work is that the problem is transformed into the modal/frequency domain, allowing absorption of sound by an inlet duct acoustic liner to be more easily included in the prediction method. An engineering numerical model, termed the frequency domain numerical solution or FDNS, has been developed. The FDNS calculates the nonlinear propagation of the rotor-alone pressure field in either a rigid or lined inlet duct. This predicts the amplitude of the rotor-alone EO tones, which dominate the buzz-saw noise signature. Note that the FDNS does not predict the initial rotor-alone pressure field (sawtooth waveform) at the fan plane: it is only a propagation model. The initial sawtooth waveform could be obtained by experimental measurement or computational fluid dynamics. Alternatively, an approximate sawtooth can be constructed by following the set-up procedure described in detail in Ref. [7, Section 3.2, pp. 137–140].

The development of the FDNS method is outlined in detail in Refs. [7,10]. In Ref. [7] the basic theory is outlined, together with some preliminary results that demonstrate the feasibility of using this method for buzz-saw noise predictions. These results show predictions of the EO frequency spectrum, compared with measurements obtained by wall-mounted microphones inside a model turbofan inlet duct. The inlet duct was rigid. At this time, experimental measurements of buzz-saw noise in an acoustically-lined duct were not available to be used for validation of the numerical method. Subsequently, in Ref. [10] the FDNS method was developed further, with modifications proposed to improve the accuracy of the prediction scheme. The objective was to develop FDNS to be used for buzz-saw noise predictions in a lined inlet duct.

During the recent European Community X-noise research project RESOUND (*Reduction of Engine SOurce Noise through Understanding and Novel Design*), coordinated by Rolls–Royce, noise measurements from a model fan rig were carried out. The experimental data which has been obtained includes measurements from in-duct wall mounted microphones. Measurements were obtained in both rigid and lined inlet ducts, over a wide range of fan operating speeds. This experimental data, particularly the measurements from the lined duct, has provided an extensive database which has been utilized.

This article contains comparisons between measurement and prediction of buzz-saw noise in a rigid and a lined inlet duct. To the authors knowledge, this is the first paper that includes both measurement and prediction of the buzz-saw EO frequency spectrum in an acoustically-lined turbofan inlet duct. The measurements presented in this article reveal the effect of an acoustic lining, at different supersonic fan speeds, on the buzz-saw noise. All the numerical simulation results that are presented in this paper have been calculated by using the new FDNS method that is detailed in Ref. [10].[4] In this article the suitability of the numerical model to be used to provide

[4]In Ref. [10] the new FDNS method is called FDNS(2).

realistic noise predictions for supersonic ducted fans is discussed, but a detailed assessment of the accuracy of the numerical method will be in a subsequent article on the prediction of buzz-saw noise.

2. Experimental measurements

During the RESOUND project Rolls–Royce tested two model fans at the Ansty Noise Compressor Test Facility (ANCTF). The first fan operated with a standard fan tip speed, and was used as the datum. The second fan was a novel design which had a reduced fan tip speed. It is measurements from the more conventional datum fan that are included in this paper. Details of the fan design and test have been reported by Bewick et al. [11], so only brief details are included in this article.

The model fan rig is representative of a modern wide-chord high-bypass-ratio engine. The fan had $B = 26$ fan blades, 58 engine section stators and 58 bypass outlet guide vanes. The duct radius at the fan plane $b = 0.44$ m, and the length of the inlet duct L is about 0.5 m. The maximum fan design speed (100%) is 10,198 rev/min. Therefore, on assuming the speed of sound $c_0 = 340$ m/s, the fan tip speed is sonic, i.e. $M_t = 1$, at about 7450 rev/min. Therefore, fan speeds that exceed 73% are supersonic.

Tests were performed with both a rigid and an acoustically-lined inlet duct. The lined inlet duct had a locally-reacting cavity lining of length l. The lining is a single-layer honeycomb structure of depth h, covered by a porous facing sheet. This is a common type of locally-reacting lining used in turbofan ducts.[5] The face-sheet was comprised of two sections with different porosities. This change in porosity is used to model the difference between the fancase and inlet liners that are commonly used in a turbofan inlet duct. (Note that the length of the fancase liner is much shorter compared with the inlet liner.) The model fancase liner had 8 thin splices, whilst the inlet liner only had 2 splices. The splices are acoustically "hard" and can cause acoustic scattering: their relevance to fan noise is discussed in Section 4.

The rigid and lined inlet ducts are shown sketched *not to scale* in Fig. 3. The full rig for these static tests also included an additional duct section, fitted at the end of the inlet duct, that contained a rotating microphone array, an intake flare and a turbulence control screen. There were four axial measuring stations located in the inlet duct, where microphones (Kulite pressure transducers) were mounted flush to the duct wall. In the lined duct, the microphones were embedded in the lining. These microphones are referred to as Kulites 1, 2, 3 and 4. Kulite 1 is located closest to the fan. Kulite 4 is located near the end of the inlet duct. The axial location of the microphones is the same in both the rigid and lined ducts. (In the lined duct some additional measurements were also obtained using a mode detection array that was located at the end of the inlet duct.)

The testing at the Rolls–Royce ANCTF was carried out in a large anechoic chamber. The fan was tested over a range of fan speeds from about 95% to 40%, (noise results were obtained during fan decelerations). Data from the in-duct microphones was analysed to evaluate the SPL EO frequency spectrum at the duct wall.

[5]This lining is known as a single degree of freedom (Sdof) liner.

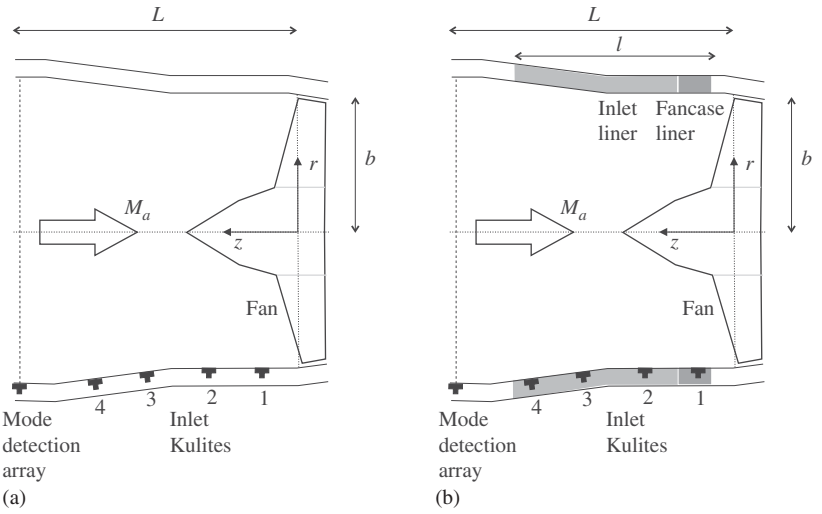

Fig. 3. Sketch of the Rolls–Royce RESOUND model fan rig and inlet duct. (a) Rigid inlet duct, (b) lined inlet duct. (Not to scale.)

Table 1
Rolls–Royce RESOUND Datum fan—supersonic fan speed test cases A–G

Case	Fan speed (%)	M_t	M_a	M_{rel}	BPF (Hz)	kb
A	75	1.03	0.41	1.11	3331	26.8
B	78	1.07	0.43	1.15	3457	27.8
C	81	1.10	0.45	1.19	3565	28.7
D	83	1.14	0.47	1.23	3682	29.6
E	86	1.18	0.49	1.28	3805	30.6
F	89	1.21	0.51	1.31	3911	31.5
G	91	1.24	0.53	1.35	4012	32.2

In this article, measurements taken at a series of different supersonic fan speeds, ranging from 75 % to 91%, are presented. The cases, named A–G, are listed in Table 1. The fan speed (%), Mach numbers (M_t, M_a and M_{rel}), BPF and kb are all listed in Table 1. M_a is the axial Mach number of the mean flow, and $M_{\text{rel}} = \sqrt{M_a^2 + M_t^2}$ is the relative Mach number of the flow impinging on the fan blades. Note that the axial Mach number M_a is assumed to be approximately constant over the duct cross-section, and the values listed are estimates of M_a close to the fan.

3. Theory

3.1. Nonlinear propagation

The basis of the nonlinear propagation model is that the rotor-alone pressure field is modelled approximately by a one-dimensional irregular sawtooth pressure waveform. The periodic

sawtooth waveform is expressed in terms of a complex Fourier series

$$P(X,T)=\sum_{m=-\infty}^{\infty} C_m(T)\,\mathrm{e}^{\mathrm{i}mX}, \tag{1}$$

where P is the non-dimensional pressure at X and T, X is a non-dimensional spatial coordinate (in a direction normal to the shock fronts, see Fig. 1), and T is the "time of flight" defined by

$$T=\frac{zB}{2\pi b}\frac{M_{\mathrm{rel}}^4}{\sqrt{M_{\mathrm{rel}}^2-1}}\left(M_a\sqrt{M_{\mathrm{rel}}^2-1}-M_t\right)^{-2}. \tag{2}$$

Eq. (2) relates the time of flight of a wave spiralling around a cylindrical duct in terms of the axial distance z propagated upstream of the fan. Eq. (2) was originally derived by Morfey and Fisher [8]. (Note in Ref. [8] it is understood that $M_a>0$ is used in Eq. (2). However, in the duct acoustics theory that is outlined in this article it is important to use $M_a<0$ to specify an inlet duct problem because the sound is propagating against the direction of the mean flow.)

In Eq. (1) each Fourier mode is equivalent to a rotor-alone EO mode, i.e. $m=\mathrm{EO}$. Having constructed a suitable initial sawtooth waveform, the initial values of the Fourier coefficients (C_m) can be determined. Then the propagation of the waveform is calculated by using a one-dimensional nonlinear wave equation. It has been demonstrated in Ref. [10] that Burgers equation is the correct equation to use.

The key step in this work is that the problem is transformed into the modal/frequency domain, and then a *linear* absorption term is added to Burgers equation. This term enables absorption of sound by an acoustic liner to be included in the simulation, based on linear decay rates of modes propagating in a lined duct. The decay rate of each of the rotor-alone EO modes is determined separately, see Sections 3.2 and 3.3.

In the frequency domain the modified Burgers equation (from Refs. [7,10]) is

$$\frac{\mathrm{d}C_m}{\mathrm{d}T}=-\frac{\mathrm{i}m\pi}{B}\left(\sum_{l=1}^{m-1}C_{m-l}C_l+2\sum_{l=m+1}^{N}C_l\widetilde{C}_{l-m}\right)-\epsilon\frac{m^2}{B^2}C_m-\sigma(m)C_m. \tag{3}$$

Eq. (3) is integrated by using a fourth-order Runge–Kutta numerical integration scheme, to evaluate the Fourier coefficients $C_m(T)$. Then, the pressure waveform at each axial station in the duct can be found by using Eq. (2) that relates T and z.

In Eq. (3) the numerical dissipation term ($-\epsilon m^2 C_m/B^2$) is required because the Fourier series is truncated at the $m=N$th term. Note that ϵ is not a constant, as clearly it must depend on the choice of N. A suitable form for ϵ is derived in Ref. [10]. The linear absorption term $-\sigma(m)C_m$ specifies the decay rate of each of the rotor-alone EO modes, and is calculated separately by using duct acoustics theory.

3.2. Duct acoustics

For a cylindrical duct containing a uniform axial flow M_a, it is well known that on assuming a harmonic acoustic pressure field $p(r,\theta,z,t)=\hat{p}(r,\theta,z)\exp(\mathrm{i}\omega t)$, solutions of the convected

Helmholtz equation can be expressed in terms of Fourier–Bessel modes

$$\hat{p}_{m,n}(r,\theta,z) = A_{m,n}J_m(\kappa_{m,n}r)\,\mathrm{e}^{\mathrm{i}(-k_{zm,n}z\pm m\theta)}, \tag{4}$$

where $A_{m,n}$ is a constant, and J_m is a Bessel function of the first kind of order m. The modes have azimuthal and axial wavenumber m and $k_{zm,n}$, respectively. The radial wavenumbers $\kappa_{m,n}$ are the resulting eigenvalues of the problem that is obtained by combining Eq. (4) with the duct wall boundary condition. For a lined duct κ and k_z are complex.

In Ref. [10] it is proposed that for each azimuthal mode m, the decay rate $\sigma(m)$ is based on the least attenuated radial mode order. Therefore

$$\sigma(m) = \mathrm{Re}\left\{\frac{\mathrm{i}k_z D}{K}\right\} = -\frac{k_{zi}D}{K}, \tag{5}$$

where $k_z = k_{zr} + \mathrm{i}k_{zi}$ is the axial wavenumber of the least attenuated mode, D is the duct diameter, and K is a constant, re-writing Eq. (2) as $T = (z/D)K$. In Ref. [12] a numerical procedure is outlined to solve the eigenvalue problem. It is important to ensure that all the modes have been located. With a lined flow duct, Rienstra [13] has shown that at a fixed frequency there can be up to four surface wave modes present. Rienstra proposes a procedure to ensure that the surface wave modes have been correctly identified.

The one-dimensional description of the rotor-alone pressure field does not include any radial dependence. It is assumed that the rotor-alone pressure field is a localized field in the region where the flow is supersonic, i.e. close to the duct wall. In terms of duct modes, this is consistent with assuming that most of the energy is in modes with radial order $n = 1$. Also, in a lined duct it is assumed that the least attenuated mode will normally be $n = 1$.

The (non-dimensional) specific acoustic impedance Z of the acoustic lining is assumed to be

$$Z = R + \mathrm{i}(X_m + X_c). \tag{6}$$

Motsinger and Kraft [14] suggest the following estimates for the resistance R, the mass reactance X_m and the cavity reactance X_c:

$$R = \frac{0.3M_a}{\rho}, \tag{7}$$

$$X_m = \frac{k(t+\varepsilon d)}{\rho}, \tag{8}$$

$$X_c = -\cot(kh). \tag{9}$$

Note that t is the face-sheet thickness, d is the diameter of the holes in the face-sheet, and ε is a dimensionless end-correction. With a significant grazing flow ε is small, and it is assumed that $X_m \approx kt/\rho$. Note that for a cavity liner there will be anti-resonance frequencies as $\cot(kh) \to \pm\infty$, i.e. $\tan(kh) = 0$. At these frequencies there will be little or no sound absorption, and the duct wall is effectively hard.

Changes in the duct's wall impedance can cause acoustic scattering; for example, at the start and end of the acoustic liner. However, in this case, as a result of using two types of facing sheet with different porosities, this could also potentially cause acoustic scattering. (These

are used to model the fancase and inlet liners.) In order to assess the accuracy of using a decay rate based on a single mode, that neglects any scattering, a more sophisticated method to calculate transmission losses in a lined duct has been considered, namely the well-known mode-matching technique.

3.3. Mode-matching

In this section the validity of basing the $\sigma(m)$'s in Eq. (3) on the decay rates of the least attenuated modes is examined in more detail. The transmission loss of the least attenuated mode in a lined duct is given by

$$\Delta_{\mathrm{LAM}} = -20k_{zi}\, l \log_{10} e, \tag{10}$$

per length l. This transmission loss is based on the assumptions that there are no duct terminations that cause reflections, or changes in the wall impedance that could cause scattering.

A more realistic model of a lined inlet duct is a cylindrical duct containing a *finite* length of acoustic lining. Also, changes in impedance can be included to model different types of liners. The mode-matching technique assumes that in each section of the duct, where the wall impedance is uniform, the sound field can be represented by a superposition of modes. Scattering of energy between the modes occurs where there is a change in impedance. Assuming the duct is axisymmetric, for fixed azimuthal mode order m, energy can only be scattered between different radial mode orders. The sound power transmission loss (Δ_{PWL}) can be calculated using mode-matching. This provides an improved measure of the absorption of acoustic energy by the liner, compared with Δ_{LAM}.

Fig. 4 illustrates the mode-matching procedure, applied to the model lined inlet duct sketched in Fig. 3b. In this case the duct is divided into four sections: I, II, III and IV. In each section the sound field is represented by a superposition of left-running (+) and right-running (−) modes. The

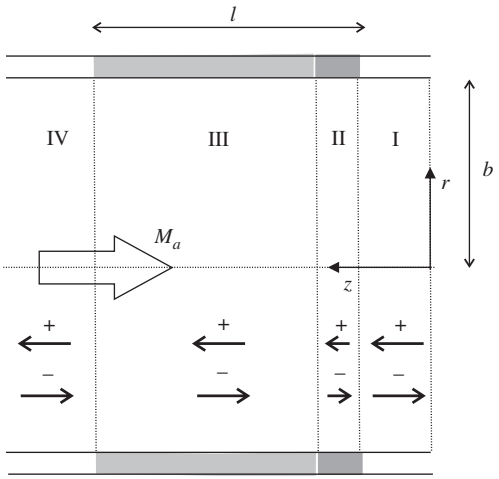

Fig. 4. Mode-matching set-up, based on the Rolls–Royce RESOUND lined inlet duct.

acoustic pressure in section $\square$ is given by

$$\hat{p}_m^{\square}(r,\theta,z) = \sum_{n=1}^{\infty} (A_{m,n}^{\square} J_m(\kappa_{m,n}^{\square+} r)\, \mathrm{e}^{-\mathrm{i}k_{z_{m,n}}^{\square+} z} + B_{m,n}^{\square} J_m(\kappa_{m,n}^{\square-} r)\, \mathrm{e}^{-\mathrm{i}k_{z_{m,n}}^{\square-} z})\, \mathrm{e}^{\mathrm{i}m\theta} \tag{11}$$

for azimuthal mode order m.

The coefficients $A_{m,n}^{\square}$ and $B_{m,n}^{\square}$, $\square = \mathrm{I} \to \mathrm{IV}$, are evaluated by following a well-known mode-matching method. For example, details of similar mode-matching schemes are outlined in Refs. [15, Chapter 2], [16–18].

$A_{m,n}^{\mathrm{I}}$ specifies the amplitude of mode (m,n) at the fan plane $z = 0$. At the fan plane the rotor-alone field is modelled by modes $(m,1)$, with $m = \mathrm{EO}$. Higher radial mode orders are neglected. Therefore, for each $m = \mathrm{EO}$ it is assumed that $A_{m,1}^{\mathrm{I}} = 1$, and $A_{m,n}^{\mathrm{I}} = 0$, $n \geqslant 2$. It is also assumed that at the end of the duct there is an anechoic termination, so all the coefficients $B_{m,n}^{\mathrm{IV}} = 0$. In order to evaluate the coefficients $A_{m,n}^{\mathrm{II}}, A_{m,n}^{\mathrm{III}}, A_{m,n}^{\mathrm{IV}}, B_{m,n}^{\mathrm{I}}, B_{m,n}^{\mathrm{II}}$ and $B_{m,n}^{\mathrm{III}}$, the harmonic acoustic pressure $\hat{p}$ and axial particle velocity $\hat{u}_z$ are matched at each location where there is a change in the wall impedance. The Galerkin method of weighted residuals is used for the matching. Therefore, at each matching plane, say $z = z_i$,

$$\int_{r=0}^{b} w[\hat{p}(r,\theta,z_i^+) - \hat{p}(r,\theta,z_i^-)]\,\mathrm{d}r = 0, \tag{12}$$

$$\int_{r=0}^{b} w[\hat{u}_z(r,\theta,z_i^+) - \hat{u}_z(r,\theta,z_i^-)]\,\mathrm{d}r = 0. \tag{13}$$

This leads to six sets of equations to evaluate the six sets of unknown coefficients. The weighting functions w are $rJ_m(\kappa_{m,n}r)$, where $\kappa_{m,n}$ are the radial eigenvalues in a rigid duct. Eqs. (12) and (13) can be simplified by making use of the orthogonality of the mode shapes in a rigid duct. Then, an iterative scheme is used to solve the set of equations, see Ref. [18].

The modal sound power $W_{m,n}$ is given by

$$W_{m,n}^{\pm} = \int_{r=0}^{b} \int_{\theta=0}^{2\pi} I_{z_{m,n}}^{\pm} r\,\mathrm{d}r\,\mathrm{d}\theta, \tag{14}$$

i.e. the integral of the modal acoustic intensity $I_{z_{m,n}}^{\pm}$ in the $\pm z$-direction, over the cross-sectional area of the duct. The form of the modal acoustic intensity used is given by Morfey [19, Eq. (16), p. 39].

In the rigid duct sections I and IV, at a fixed frequency, the power in each mode can be summed because the mode shapes are orthogonal. Define $W_m^+ = \sum_n W_{m,n}^+$, where the summation is over all the left-running (+) cut-on radial mode orders. Then, for azimuthal mode order m the sound power transmission loss is

$$\Delta_{\mathrm{PWL}} = 10 \log_{10} \frac{W_m^+|_{\mathrm{I}}}{W_m^+|_{\mathrm{IV}}}. \tag{15}$$

Fig. 5 shows a comparison of Δ_{PWL} and Δ_{LAM} for rotor-alone EO modes, for $m = \mathrm{EO} = 1$ to $4B$. Cases A, C, E and G are shown, see Table 1. Note that if mode $(m,1)$ is cut-off, then Δ_{PWL} is zero. The calculation of Δ_{PWL} includes the effect of any scattering at the junctions between the different duct sections. However, as the length of the fancase lining is very short, the Δ_{LAM}

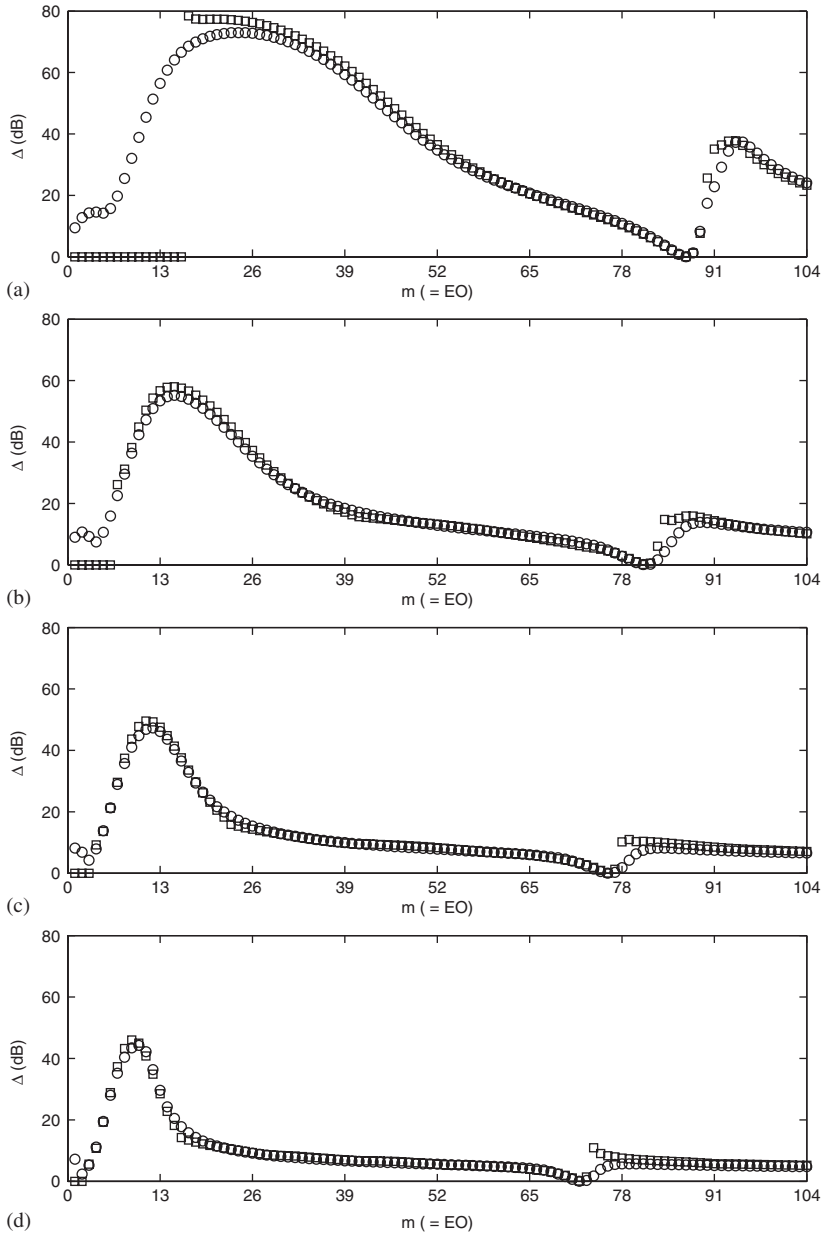

Fig. 5. Comparison between predicted sound power and least attenuated mode transmission loss (□, Δ_{PWL}; ◯, Δ_{LAM}) for rotor-alone EO modes $m = EO = 1$ to $4B$: (a) Case A; (b) Case C; (c) Case E; and (d) Case G.

calculation is only based on a uniform liner of length l, with the same acoustic impedance as the inlet lining. This simplifies the calculation of Δ_{LAM}.

In each case there appears to be little difference between the two predicted transmission losses. It appears that realistic values for $\sigma(m)$ can be determined based only on the least attenuated

mode, without having to use a more sophisticated approach such as mode-matching. Therefore, all the FDNS simulations (for a lined inlet duct) in Section 4 have used values for $\sigma(m)$ calculated by determining Δ_{LAM}.

Note that the transmission losses are predicted to change at different fan speeds. For example, compare Case A 75% with Case G 91% in Fig. 5. The reason for this is discussed in Section 4.

4. Comparison of measurement with prediction

A comparison of measurement with prediction of the buzz-saw EO frequency spectrum, at different supersonic fan speeds, has been performed. The fan speeds, referred to as cases A–G, are listed in Table 1. Results have been obtained for a rigid and an acoustically-lined inlet duct. The two main objectives of this study are an assessment of the effect of an acoustic liner on buzz-saw noise, and an assessment of the accuracy of the numerical simulations by validation with experimental measurements.

4.1. Measurements close to the fan

It is assumed that close to the fan the rotor-alone pressure field, near the duct wall where the flow onto the fan blades is supersonic, can be modelled by a one-dimensional irregular sawtooth pressure waveform. The first step in the simulation method is to construct an initial sawtooth waveform that approximates the rotor-alone pressure field close to the fan. In Ref. [7] a set-up procedure is outlined. This can be used to construct a sawtooth waveform from an estimate of the initial levels of the low-order EO tones. Measurement of the full EO frequency spectrum close to the fan is not required. An example of a typical estimate of an irregular sawtooth, and its EO frequency spectrum, is shown in Fig. 6. Note that it is assumed that the sawtooth has well-defined shocks. This implicitly means that the EO frequency spectrum should contain high-amplitude tone levels at high frequencies.

It is important to start the numerical simulation near the fan, where the SPLs are close to their highest level. This is because in this region, nonlinear propagation will modify the pressure waveform. However, in the model inlet duct no Kulites are positioned adjacent to the fan, see Fig. 3. At Kulite 1, the sawtooth waveform may already have been modified, compared with the type of waveform close to the fan.

Fig. 7 shows the measured EO frequency spectrum at Kulite 1, in the rigid inlet duct, for cases A–G. Similarly, Fig. 8 shows the measured EO frequency spectrum at Kulite 1, in the lined inlet duct, for cases A–G. First, compare the spectra measured at Kulite 1 in the rigid and lined inlet ducts. They are similar, but not identical. The small differences in the two sets of spectral measurements (at Kulite 1) are assumed to be due to several factors. Firstly, in general the tone levels at Kulite 1 are slightly lower in the lined duct because the microphone is situated slightly upstream of the start of the lining. Secondly, wall measurements in a lined duct may also be lower, because the pressure maximum in the first radial order's mode shape is not located at the wall in a lined duct. Thirdly, the test conditions may have varied slightly between testing the rigid and lined inlet ducts.

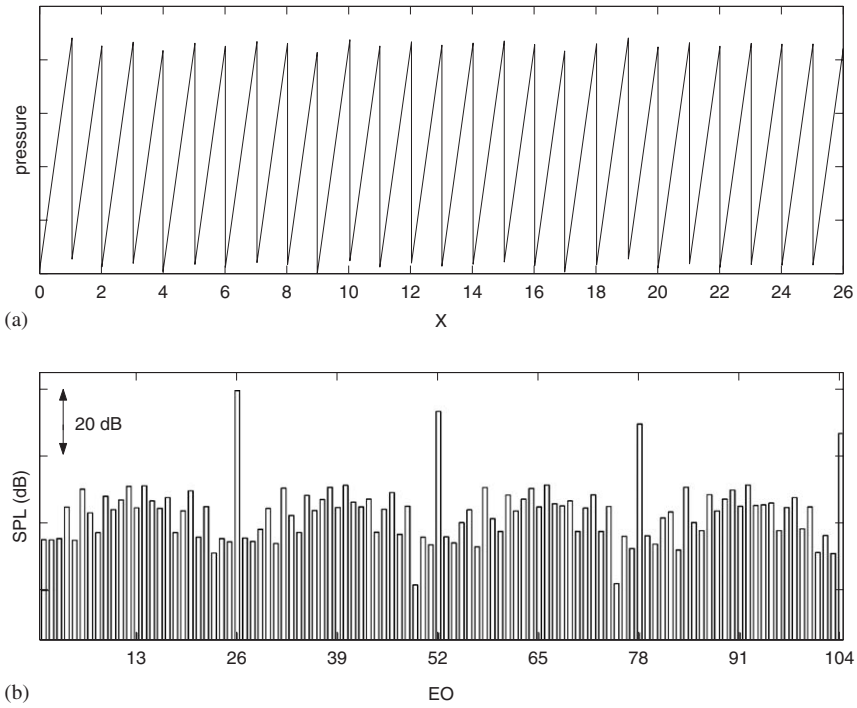

Fig. 6. Example of a (theoretical) irregular sawtooth pressure waveform close to the fan: (a) pressure waveform; (b) EO frequency spectrum. Note in this example the fan has 26 rotor blades.

Next, compare the spectra in Figs. 7 and 8 with the theoretical spectrum shown in Fig. 6(b). In general, for both sets of measurements the EO frequency spectrum changes subtly with increasing fan speed. At low supersonic fan speeds, each measured spectrum is qualitatively similar to the theoretical spectrum, e.g. compare Figs. 7(a)–(c) and 8(a)–(c) with Fig. 6(b). However, at high supersonic fan speeds it is noticeable that the measured tone levels at high-order EOs are up to 10 dB less than their corresponding levels at lower fan speeds. The shocks in the pressure waveform are likely to be less well-defined at high fan speeds. This observation was also reported in Ref. [7], with measurements from another fan rig.

In Ref. [7] it is commented that at high supersonic fan speeds, the shock strength at the duct wall may be reduced, due to the onset of shock swallowing that can occur at high speeds close to the fan's maximum design speed. Also, at high fan speeds three-dimensional effects may be more significant, because additional higher radial mode orders cut on, which could affect measurements at the duct wall, owing to interference effects. It is important to note that the sawtooth waveform description of the rotor-alone pressure field appears to become less realistic at very high fan speeds. However, these high fan speeds are not typically an important condition for noise. The maximum Fan speed that has been used for comparison between measurement and prediction is 91%.

In this article all the simulations utilize an initial pressure waveform that has been constructed using the complete EO frequency spectrum, measured at Kulite 1, for that test case. This is in

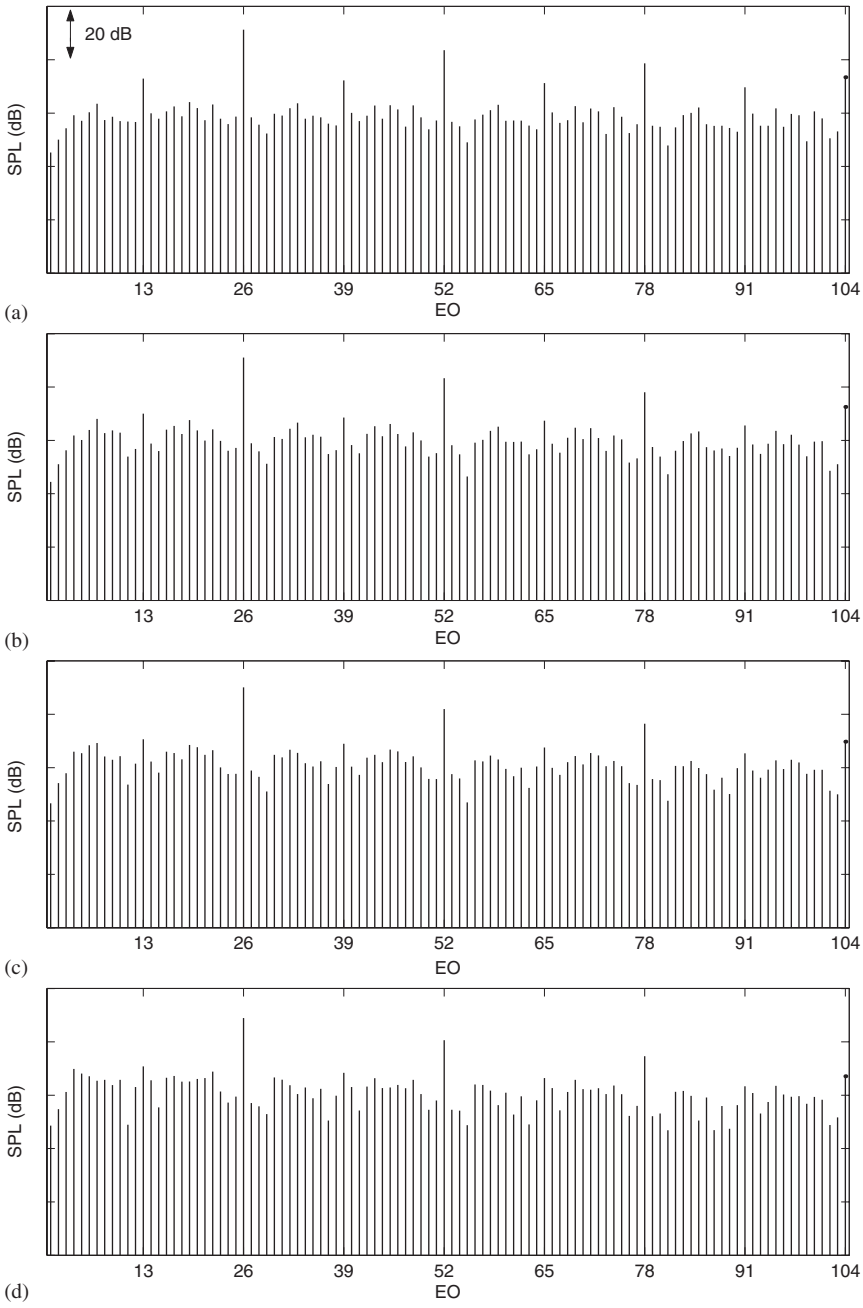

Fig. 7. Measured EO frequency spectrum at Kulite 1 in the rigid inlet duct: (a) Case A; (b) Case B; (c) Case C; (d) Case D; (e) Case E; (f) Case F; and (g) Case G.

order to reduce uncertainty owing to not having measurements very close to the fan. The measured level of each EO tone is used to specify the initial values of $|C_m|$, i.e. the amplitudes of the Fourier harmonics in Eq. (1).

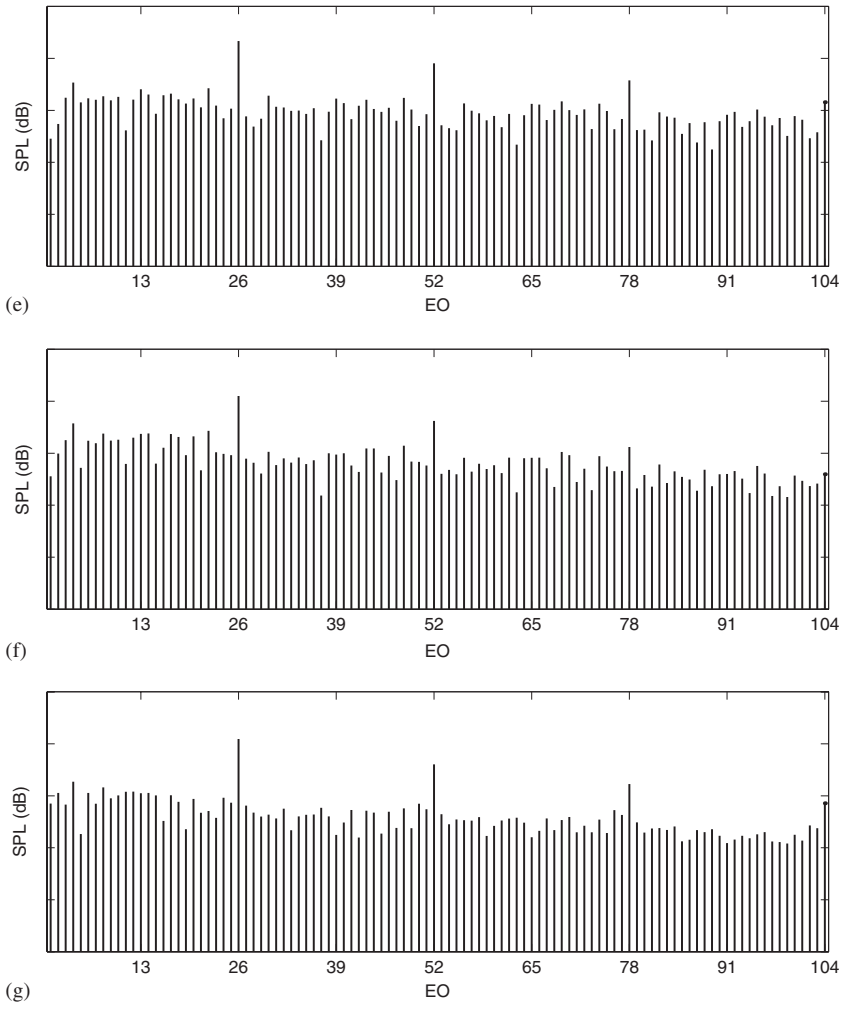

Fig. 7. (*Continued*)

In Ref. [6] the principal factor affecting the irregularity of the rotor-alone pressure field was found to be variations in the blade-to-blade stagger angles. In simplistic terms, the difference in the stagger angles affects the amplitude of the EO tones. The stagger angle variation for a complete fan blade set will not normally be known, although a practical estimate of the amplitudes could be obtained by knowing the maximum stagger angle tolerance. However, both the amplitude and phase of the EOs are required to be able to specify the initial values of the complex C_m's. The phasing can be thought of in terms of the ordering of the fan blades. Other than by direct measurement, the initial phases of the EO modes will not be known.

Owing to the phase angles being unknown, a set of numerical simulations are averaged to generate a mean prediction. Each simulation uses a different set of randomly generated phases, to be able to specify the initial values of the C_m's. The phases are assigned a random value which is uniformly distributed between 0 and 2π. In this article, all the numerical predictions have been

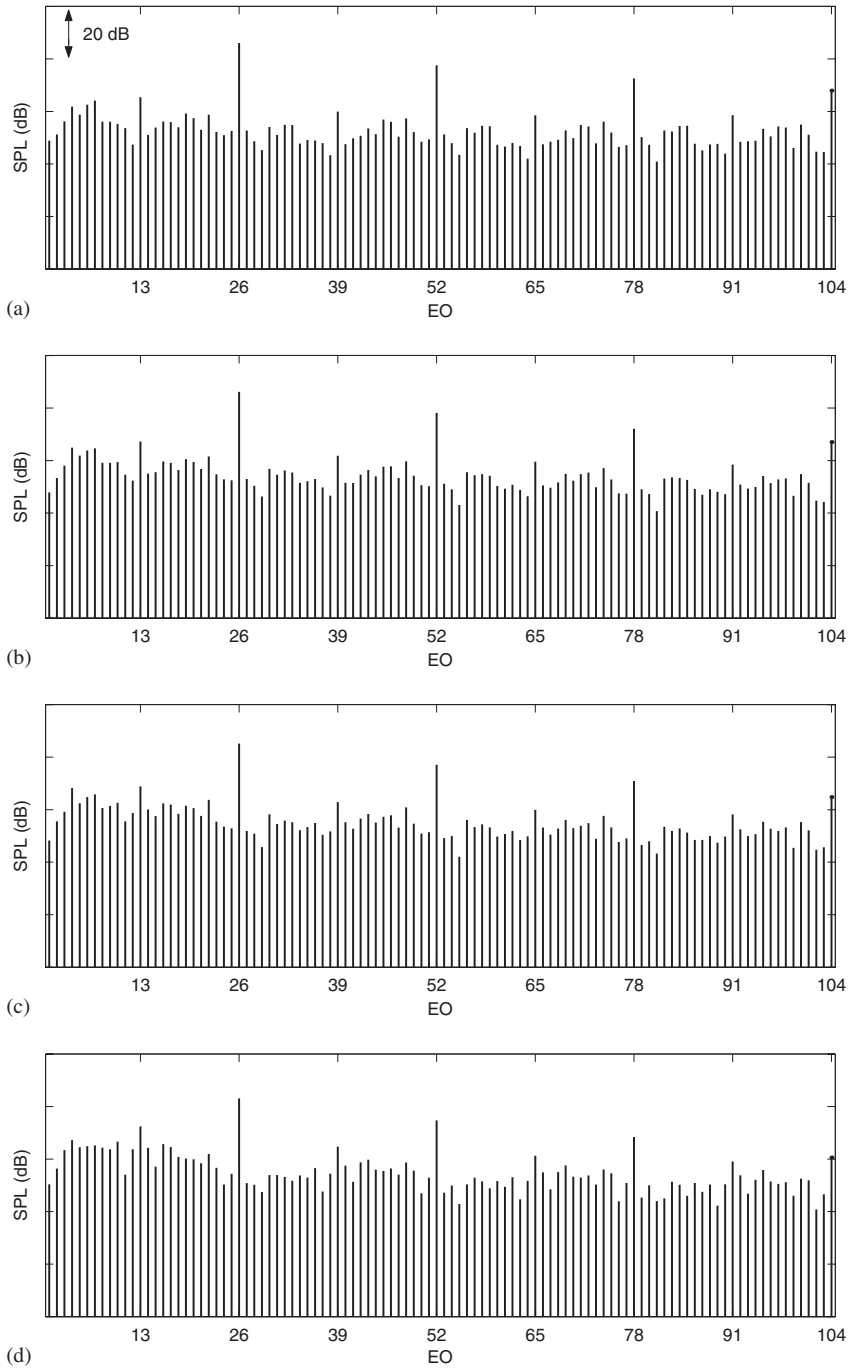

Fig. 8. Measured EO frequency spectrum at Kulite 1 in the lined inlet duct: (a) Case A; (b) Case B; (c) Case C; (d) Case D; (e) Case E; (f) Case F; and (g) Case G.

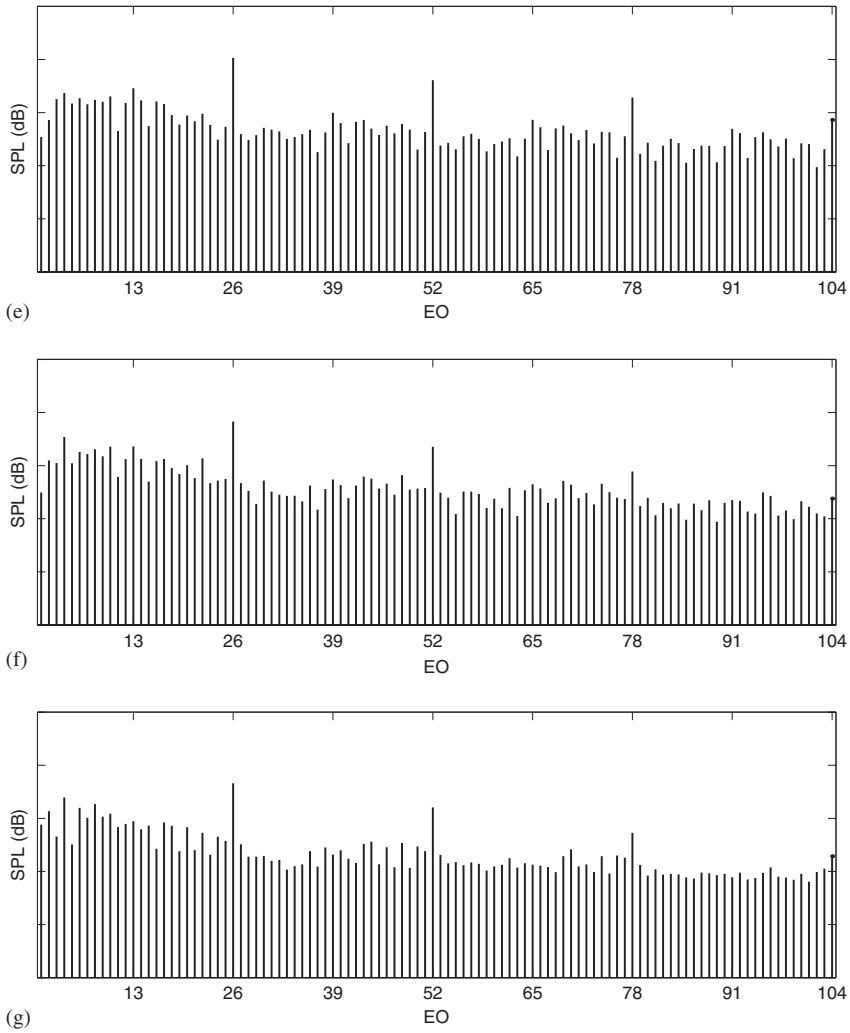

Fig. 8. (*Continued*)

calculated by averaging fifty simulations. The aim is to predict the general shape of the buzz-saw EO frequency spectrum, without necessarily being able to predict the exact level of each tone.

4.2. Results: rigid inlet duct

In Fig. 9 there is shown comparisons between measurement and prediction, for fan speed cases A–G, of the EO frequency spectrum at Kulite 4 located in the rigid inlet duct. Note that in Figs. 7–9 and 15 the same scale on the SPL axis is used, although the absolute scale is not shown. There is no liner in the duct, but in the simulations the effect of mode cut-off has been included via the absorption term, $-\sigma(m)C_m$, in Eq. (3). In general, there is good agreement between the measured and predicted levels of the EO tones at Kulite 4 in the rigid inlet duct shown in Fig. 9.

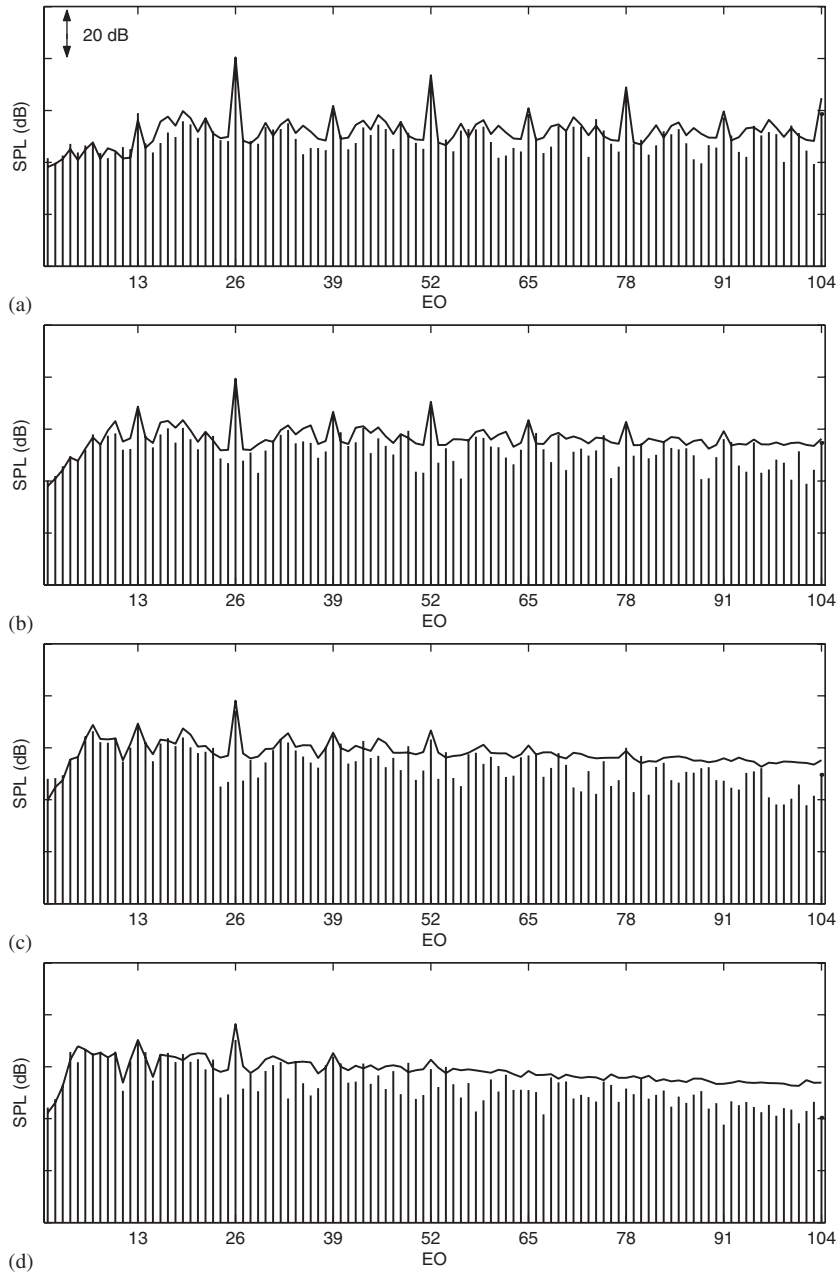

Fig. 9. Measured EO frequency spectrum at Kulite 4 in the rigid inlet duct: (a) Case A; (b) Case B; (c) Case C; (d) Case D; (e) Case E; (f) Case F; and (g) Case G. The FDNS prediction is shown by the solid line.

The effect of cut-off at low-order EOs has been successfully included in the simulations. For example, consider case A. At this low supersonic fan speed EO 1–15 are predicted to be cut-off, and the levels of these EO tones have been accurately predicted, see Fig. 9(a).

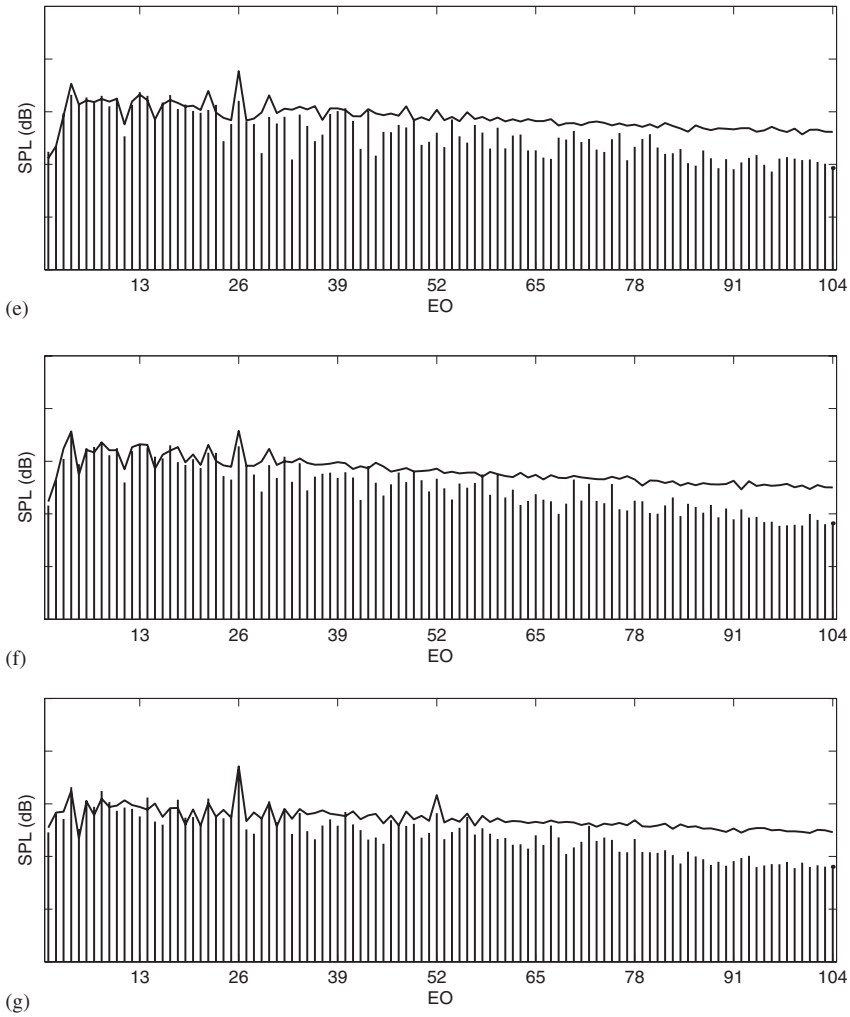

Fig. 9. (*Continued*)

The tone levels of the low-order EOs that are *not* cut-off tend to remain unchanged inside the inlet duct. However, nonlinear attenuation reduces the levels of the high-order EOs. This leads to the characteristic low-pitched buzz-saw noise signature. These trends are predicted by the simulations. The numerical results are an average of fifty simulations, so it is not surprising that the mean predictions tend to show a smoothed fit to the measured EOs, but do not accurately predict the level of each tone.

In the rigid inlet duct, the largest discrepancy between the measured and predicted tone levels is at high-order EOs for cases E, F and G. These cases are the three highest fan speed test cases. In each case there is poor agreement at $EO > 2B$, see Fig. 9(e)–(g). As noted previously, at high fan speeds the rotor-alone pressure field is likely to be more three-dimensional, notably at high-frequencies because more radial mode orders are cut on. Therefore, it is possible that the

simulation method will not be able to accurately predict the high-order EO tone levels, at high supersonic fan speeds.

Another possible explanation is that at these high frequencies there is boundary-layer "shielding", and the measured levels of the tones may be low due to refraction effects by the boundary layer at the duct wall. It is anticipated that boundary-layer shielding would only affect high-frequency sound. At high fan speeds, the frequencies of the EOs are higher owing to the increased shaft rotation frequency. The measurements at Kulite 1, which are used to construct the initial pressure waveform, may suffer less from shielding. In the region close to the fan, the flow is being accelerated (due to the fan and spinner), and the boundary-layer is likely to be thinner, compared with further upstream of the fan. At this time, the main reason for this discrepancy between measurement and prediction is not known.

4.3. Results: acoustically-lined inlet duct

Simulations for the lined inlet duct require the decay rates of the least attenuated modes to be calculated. Although only EOs up to $4B$ were measured, the FDNS simulations are not truncated until $N = 10B$. In Figs. 10–13 the least attenuated mode transmission loss Δ_{LAM} for $m = \mathrm{EO} = 1$ to $10B$ is shown for fan speed cases A, C, E and G. Note that the transmission loss is in dB per l, where l is the length of the liner. Also plotted are examples of the mode shapes. The corresponding results for fan speed cases B, D and F are not shown, but they do not show any significant changes.

In Fig. 14 an example of the specific acoustic impedance Z at fan speed case A is plotted. The resistance R and reactance X are both shown. R is constant, but X is dependent on frequency, see Eqs. (7)–(9). Comparing Figs. 10 and 14, the transmission loss is zero as $|X| \to \infty$. The first anti-resonance is at $\lambda/2 = h$, i.e. the depth of the liner cavity equals half the acoustic wavelength. For cases A–G, the liner's first anti-resonance is close to 3 BPF.

In Figs. 10–13 the predicted values of Δ_{LAM} for rotor-alone EO modes with azimuthal mode order $m = \mathrm{EO} = 1$ to $10B$ are shown for cases A, C, E and G. $\mathrm{EO} = 10B$, or 10 BPF, corresponds to a Helmholtz number kb between about 250–300. This will not be at an audio-frequency, but the simulations include frequencies up to 10 BPF.

With this type of lining, there are three anti-resonance frequencies in the frequency range up to 10 BPF. The liner is effectively acoustically hard at these anti-resonance frequencies. At each fan speed, the maximum transmission loss is predicted at a frequency less than the first anti-resonance frequency. At fan speed 75% (case A), the maximum transmission loss is at a frequency close to BPF. Increasing the fan speed reduces the value of the maximum transmission loss, and also reduces the EO at which the maximum transmission loss occurs. For example, compare case A and G, see Figs. 10 and 13.

It is well known that increasing the fan speed leads to a reduction in sound absorption in a lined duct because the rotor-alone EO modes' cut-off ratios increase with fan speed.[6] This is more easily thought of in terms of geometric acoustics. In a two-dimensional duct each mode can be expressed in terms of the sum of two plane waves. (In a cylindrical duct the modes can only be expressed

[6]Note that the term "cut-off" ratio should strictly only be used to characterize acoustic modes in a rigid duct. However, the concept of "cut-off" ratio and mode angle are useful to visualize modes in a lined duct.

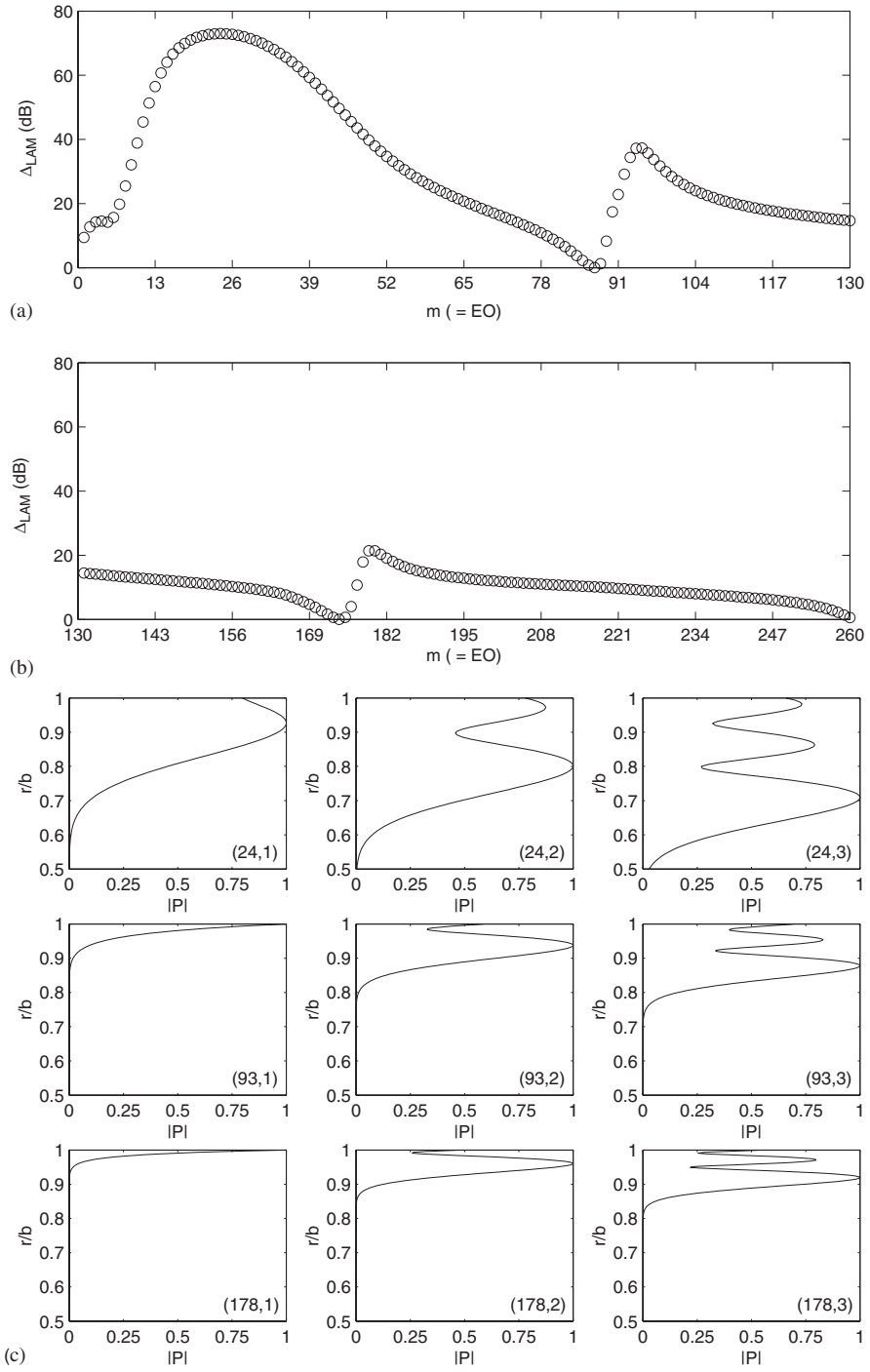

Fig. 10. Lined inlet duct—Case A: (a) Predicted decay rates of rotor-alone EO modes. Δ_{LAM} for $m = \mathrm{EO} = 1$ to $5B$. (b) Δ_{LAM} for $m = \mathrm{EO} = 5B$ to $10B$. (c) Examples of predicted mode shapes (m, n). Least attenuated modes: $m = 24, n = 1$; $m = 93, n = 2$; $m = 178, n = 2$.

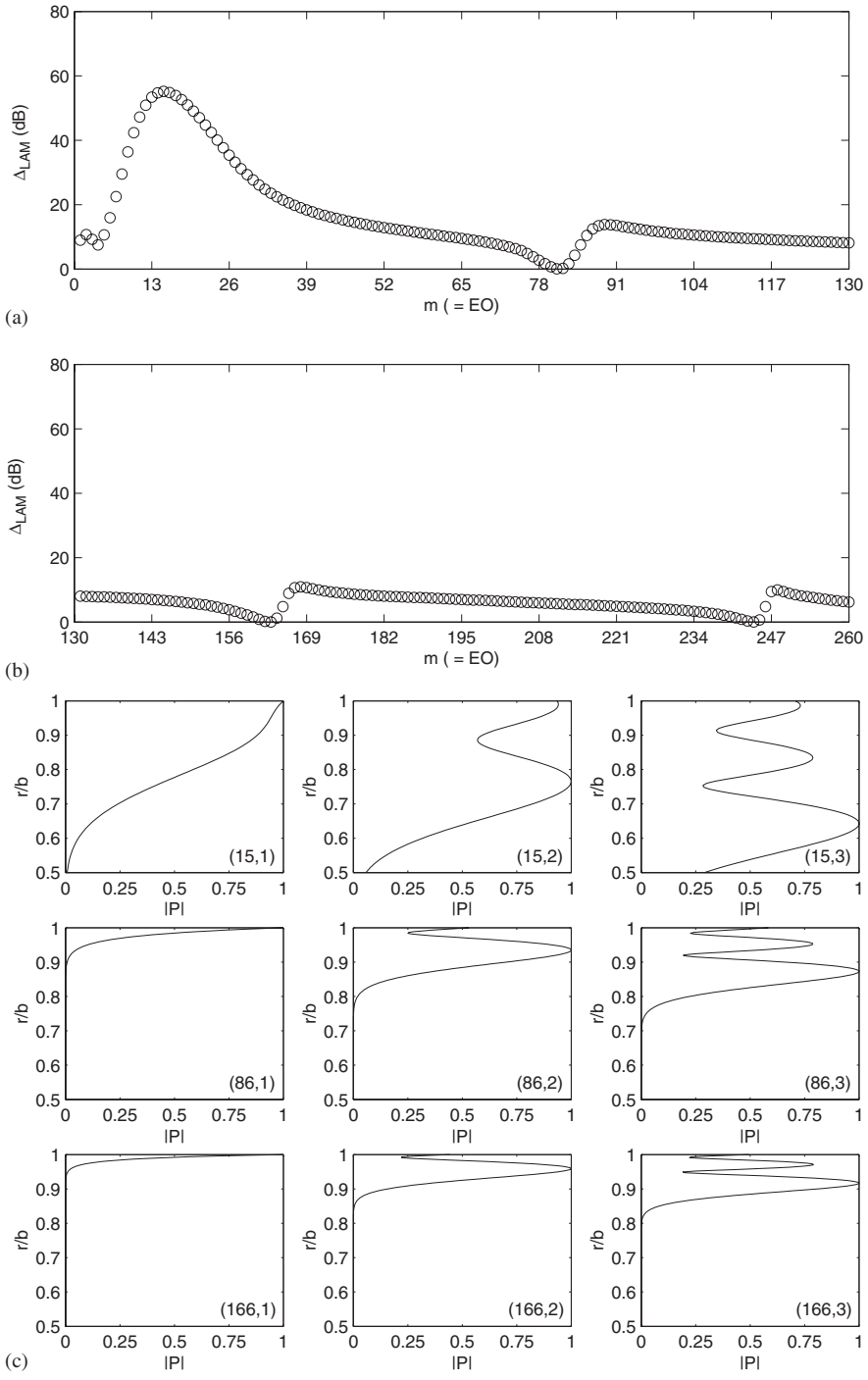

Fig. 11. Lined inlet duct—Case C: (a) Predicted decay rates of rotor-alone EO modes. Δ_{LAM} for $m = \mathrm{EO} = 1$ to $5B$. (b) Δ_{LAM} for $m = \mathrm{EO} = 5B$ to $10B$. (c) Examples of predicted mode shapes (m, n). Least attenuated modes: $m = 15, n = 1$; $m = 86, n = 2$; $m = 166, n = 2$.

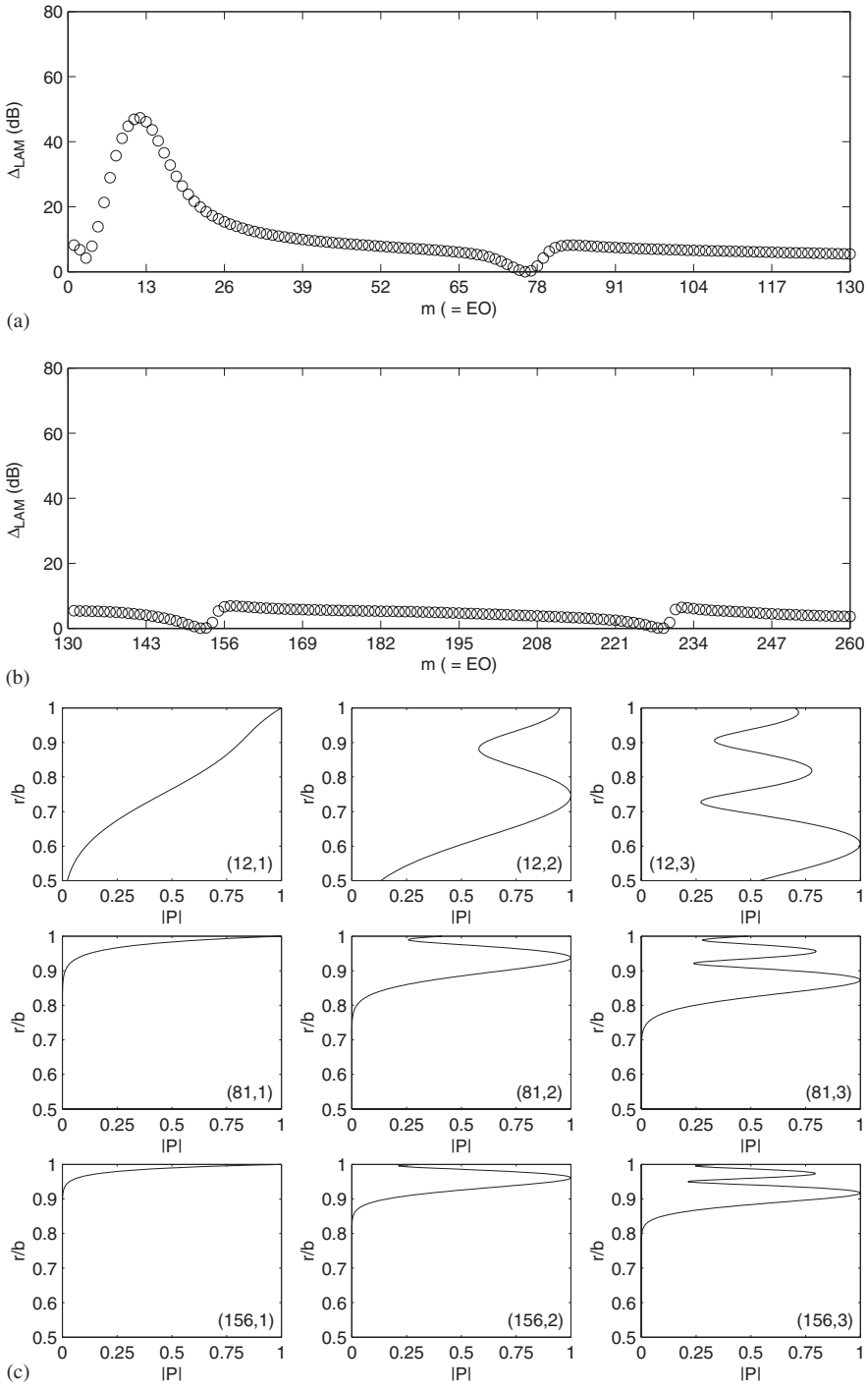

Fig. 12. Lined inlet duct—Case E: (a) Predicted decay rates of rotor-alone EO modes. Δ_{LAM} for $m = \mathrm{EO} = 1$ to $5B$. (b) Δ_{LAM} for $m = \mathrm{EO} = 5B$ to $10B$. (c) Examples of predicted mode shapes (m, n). Least attenuated modes: $m = 12, n = 1$; $m = 81, n = 2$; $m = 156, n = 2$.

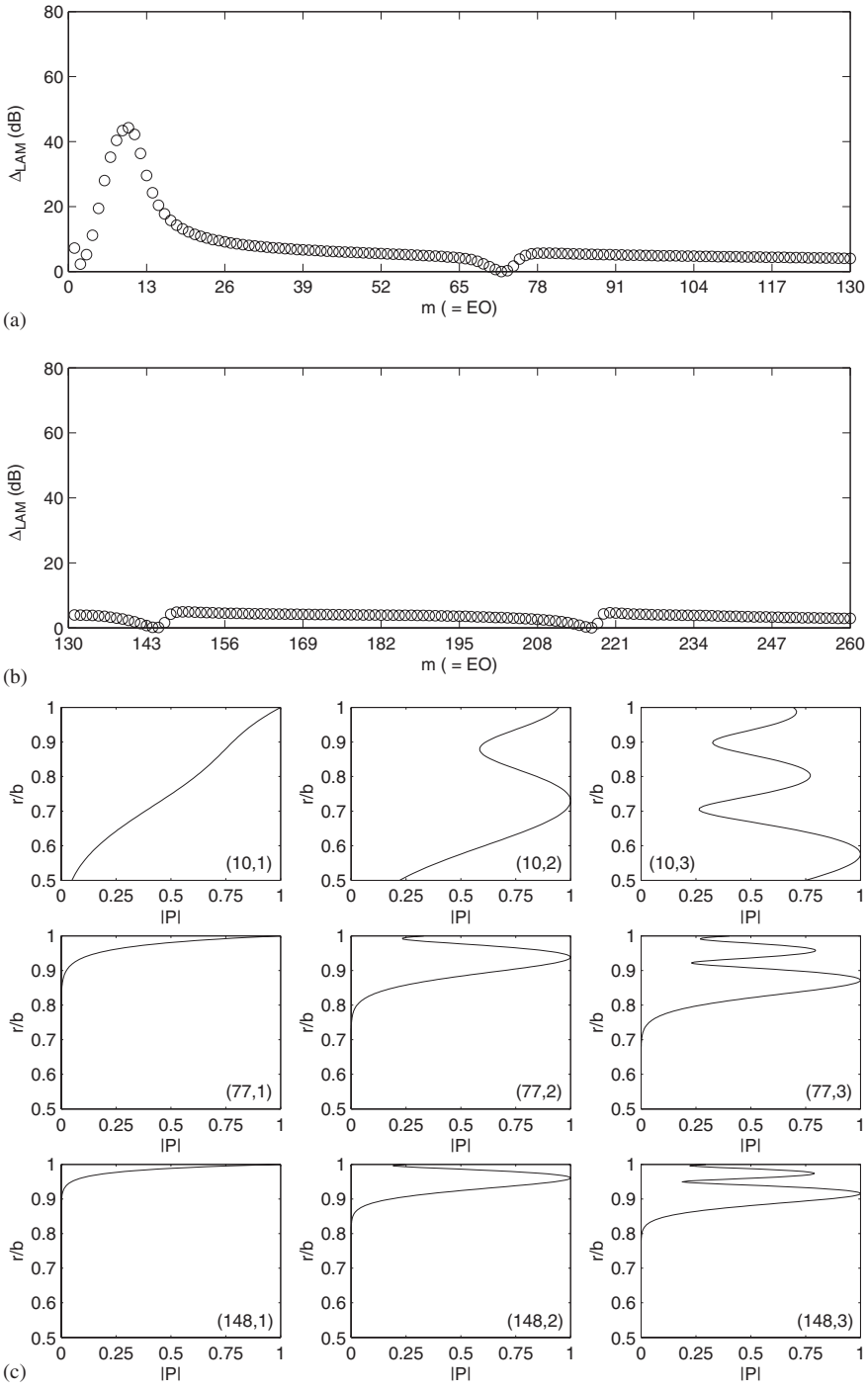

Fig. 13. Lined inlet duct—Case G: (a) Predicted decay rates of rotor-alone EO modes. Δ_{LAM} for $m = \mathrm{EO} = 1$ to $5B$. (b) Δ_{LAM} for $m = \mathrm{EO} = 5B$ to $10B$. (c) Examples of predicted mode shapes (m, n). Least attenuated modes: $m = 10, n = 1$; $m = 77, n = 2$; $m = 148, n = 2$.

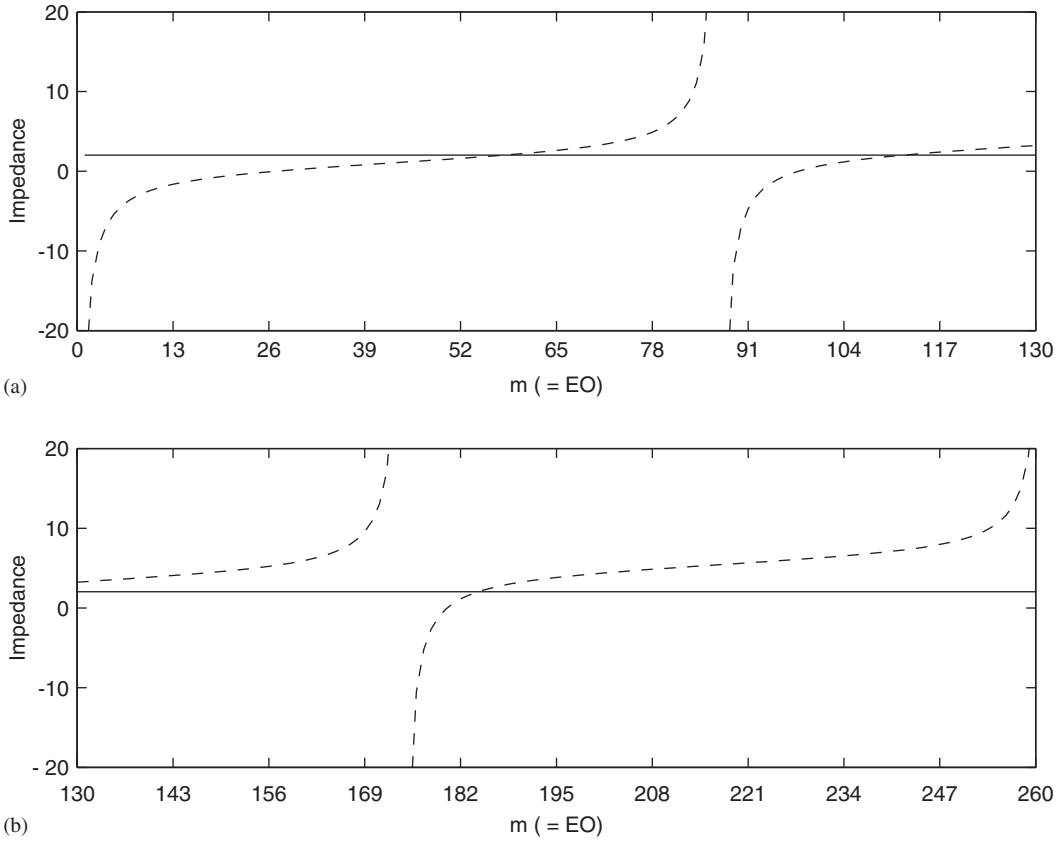

Fig. 14. Predicted specific acoustic impedance $Z = R + \mathrm{i}X$ of the acoustic liner (Case A only): —, R; - - -, X.

approximately in terms of plane waves.) The plane waves propagate in a direction that can be defined by the mode angle, that is the angle between the direction of propagation and the duct axis. A mode that is almost cut-off will have a mode angle close to 90°. Therefore, in a lined duct as this mode propagates it will be reflected many times between the duct walls, and be well absorbed by a liner. However, a well cut-on mode will have a small mode angle. Thus, as it propagates it will suffer less reflections at the duct wall, and consequently it will be less well absorbed by a liner. This simple argument illustrates that the transmission loss in a lined duct is dependent on the mode, in addition to the properties of the acoustic lining. In general, well cut-on modes that propagate in a lined duct will be poorly absorbed, regardless of the acoustic impedance of the lining.

Comparing Figs. 10 and 14 it is seen that for fan speed case A, local maximum points in the transmission loss at EO = 24, 93 and 178 each occur at an impedance with reactance $X < 0$. (Note $\mathrm{e}^{\mathrm{i}\omega t}$ is used.) Examples of the first three radial mode order shapes, for $m = 24$, 93 and 178, are also shown in Fig. 10(c). Similar examples for cases C, E and G are shown in Figs. 11–13. It is interesting to note that the least attenuated mode is not always the first radial mode order. However, there is a clear pattern that is seen in each case. If the least attenuated mode is $n = 2$, then the first radial mode order has a distinctive shape: the pressure decays very rapidly with

distance away from the duct wall. This type of mode is known as a surface wave. Rienstra [13] has shown that a surface wave's pressure decays exponentially with distance away from the wall. In Ref. [13] it is shown that surface wave modes only occur when $X<0$. The surface wave is not the least attenuated mode because these modes tend to have large axial decay rates.

Having identified and neglected any surface waves, the mode shapes associated with the least attenuated mode are in fact similar. The maximum radial pressure will always be located at, or very close to, the duct wall. This is consistent with the one-dimensional approximation, used to approximate the rotor-alone pressure field, which neglects any radial dependence in the modelling.

In a rigid duct it is straightforward to order the radial modes. The boundary condition at $r=b$ is $\partial p/\partial r=0$, i.e. the radial pressure has a turning point at the duct wall. The modes are ordered corresponding to the number of turning points in the radial pressure from the centre of the duct to the wall. In a lined duct there is no standard procedure that is used to order the radial modes. In this article, the radial modes are ordered by their number of turning points following the same procedure used for a rigid duct. Therefore, in a rigid duct the rotor-alone pressure field is thought of in terms of a superposition of only first radial mode orders. This ensures that the energy is localized at the duct wall. In a lined duct, this superposition of 'first' radial mode orders will actually be a superposition of the least attenuated modes, which to a first approximation is used to model the rotor-alone pressure field.

In Fig. 15 there is shown comparisons between measurement and prediction, for fan speed cases A–G, of the EO frequency spectrum at Kulite 4 located in the lined inlet duct. Note that in Figs. 7–9 and 15 the same scale on the SPL axis is used, although the absolute scale is not shown. The effect of an acoustic liner on buzz-saw noise, at different fan speeds, can be seen by comparing Figs. 9 and 15. In the lined inlet duct, it is low-order EOs *and* BPF that remain the dominant tones, i.e. EOs which protrude above their neighbouring tones in the frequency spectrum. Low frequencies (low-order EOs) are poorly absorbed by the acoustic lining. The BPF tone will be absorbed by the lining, but remains a dominant tone because there is less nonlinear attenuation. In the rigid duct, it is nonlinear attenuation that reduces the level of the BPF tone. However, in the lined duct, tones close to BPF tend to be well absorbed by the lining, which means BPF suffers less nonlinear attenuation because its neighbouring tones are more rapidly reduced to linear levels.

The frequency range of the EOs that are well-absorbed by the acoustic liner narrows with increasing fan speed. For example, for case A it is seen that the liner has been effective at frequencies up to about 2 BPF, e.g. compare Figs. 9(a) and 15(a). The average level of the EO tones in this range is nearly 20 dB lower in the lined duct. Now compare this with case G. The liner has only been effective in the frequency range $\frac{1}{2}$ BPF to BPF, e.g. compare Figs. 9(g) and 15(g). Outside this frequency range there is little difference between the measured EOs in either the rigid or lined inlet duct.

The measurements in the lined inlet duct demonstrate that an acoustic liner will reduce the buzz-saw noise radiated from the duct. In general, at all the fan speeds it appears that tones between $\frac{1}{2}$ BPF and BPF are well absorbed by the lining. This changes the buzz-saw signature in a lined inlet duct, because in the absence of an acoustic liner, it is these tones that tend to dominate the buzz-saw noise spectrum.

These results are the first example of predictions of the complete buzz-saw noise spectrum, compared with experimental measurements, in an acoustically-lined inlet duct. In general, the

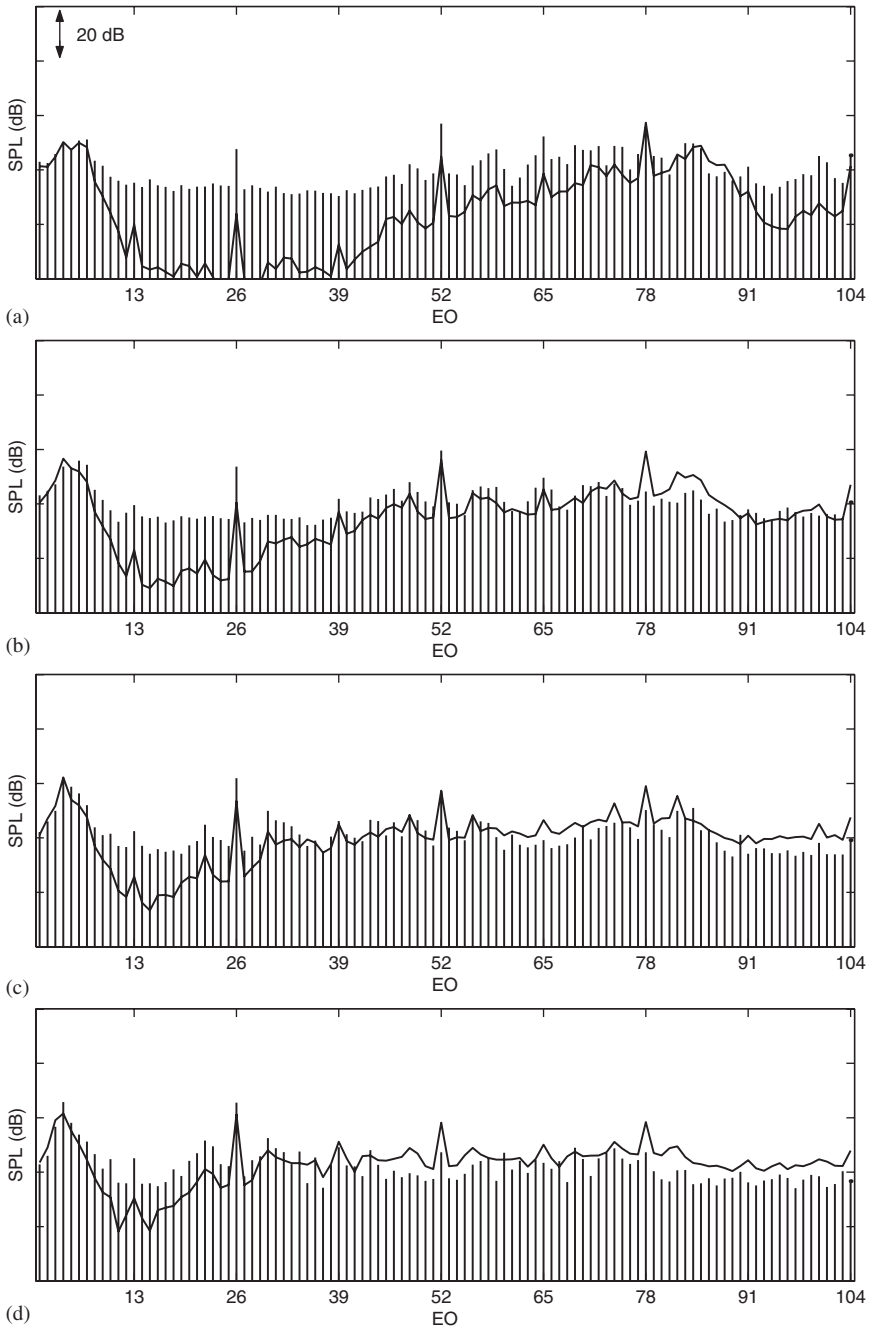

Fig. 15. Measured EO frequency spectrum at Kulite 4 in the lined inlet duct: (a) Case A; (b) Case B; (c) Case C; (d) Case D; (e) Case E; (f) Case F; and (g) Case G. The FDNS prediction is shown by the solid line.

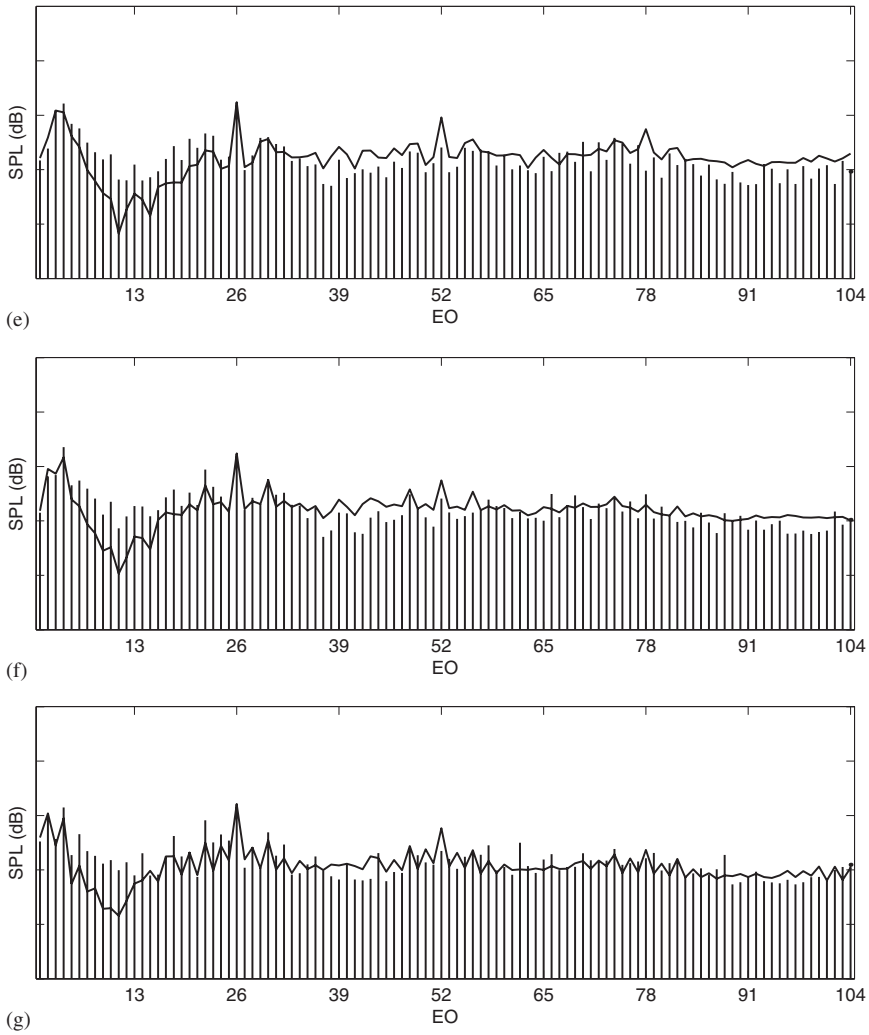

Fig. 15. (*Continued*)

agreement between measurement and prediction of the EO frequency spectrum in the lined inlet duct is not as close as the agreement seen in the results for the rigid inlet duct, e.g. compare Figs. 9 and 15. Notably at low supersonic fan speeds there appears to be very poor agreement between some of the measured and predicted levels of the EO tones. For example, for cases A and B there are differences between measurement and prediction at some EOs in excess of 30 dB, see Fig. 15(a) and (b). It is likely there are two main reasons for these large discrepancies.

Firstly, it is noticeable that at each fan speed, the largest discrepancies between the measured and predicted tone levels appear to be at EOs that are predicted to be well absorbed by the acoustic liner, e.g. compare Figs. 10–13 with 15. In the simulations the amount of absorption by the liner, notably at EOs in the liner's optimum performance frequency range, tends to be over-predicted. At these frequencies, the predicted tone levels are consistently lower than their

measured levels. It is probable that the predicted modal decay rates used in the numerical simulations, i.e. the values of $\sigma(m)$, are too high.

The duct acoustics theory used to calculate the modal decay rates is based on several assumptions: the mean flow is a uniform "plug" flow with no boundary layer; the liner's acoustic impedance can be accurately estimated in the presence of flow and high SPLs; the duct is cylindrical with constant radius.

In practice, the flow in an inlet duct is not uniform. In an inlet, sound is propagating against the oncoming flow, which means a boundary layer will refract sound away from the duct wall. Therefore, the modal decay rates predicted with the inclusion of a boundary layer, would generally be lower than the rates predicted with uniform flow.

The acoustic lining in an inlet duct is unlikely to have a uniform impedance. It is difficult to manufacture a lining that is essentially a homogeneous material, and to remain so in the harsh environment inside a turbofan inlet duct. It is also difficult to accurately predict the acoustic impedance in the presence of a grazing flow and high SPLs. Eq. (7) takes account of the mean flow, but does not include any nonlinear behaviour caused by high SPLs.

Also, modal decay rates can be linked to the concept of a mode's cut-off ratio. A mode's cut-off ratio (in a rigid duct) is defined in terms of the duct radius, axial Mach number, and frequency of the sound. However, in a real inlet the radius of the duct, and the axial Mach number are not constant. In the simulations the duct radius b and the axial Mach number M_a have been specified based on their values close to the fan. In this way the modes should be correctly specified close to the start of the acoustic lining, although no allowance is made for changes in the modes as they propagate upstream of the fan.

It is difficult to assess how realistic the predicted modal decay rates are, because of the combination of factors that could affect the overall attenuation that is achieved in practice. It is anticipated that the use of more realistic modal decay rates would improve the comparison between measurement and prediction.

There is a second reason that could explain the discrepancies in the results at low supersonic fan speeds. It is known (see Ref. [20]) that at low supersonic fan speeds the rotor-alone EO tones are not necessarily the dominant tones in the EO frequency spectrum. At these fan speeds, non-rotor-alone EO tones generated by scattering, can provide a significant contribution to the noise. The scattering is mainly caused by acoustically hard longitudinal splices, which are required to fix the lining in a turbofan inlet duct. If the levels of the scattered modes exceed the levels of the rotor-alone modes, then the FDNS prediction method is no longer valid to be used at that fan speed. This is because the assumption that the principal source of buzz-saw noise is the rotor-alone EO tones is not valid. An analysis of the measurements in the lined inlet duct, using the mode detection array, would be required to determine whether scattering has affected these results.

Finally, the validation study appears to demonstrate that at high supersonic fan speeds, in the lined duct there is reasonably good agreement between the measured and predicted EO tone levels. However, it is interesting to compare the results in the rigid and lined inlet ducts at high supersonic fan speeds, (e.g. cases E, F and G). In the rigid duct, there is a noticeable discrepancy between the measured and predicted tone levels at frequencies greater than 2 BPF, see Fig. 9(e)–(g). Contrast this with the results in the lined inlet duct, see Fig. 15(e)–(g). At high frequencies, there is no such discrepancy between the measured and predicted EO tone levels. It

has been suggested that at these high fan speeds, boundary-layer shielding at high frequencies may occur. This effect would occur in both the rigid and lined inlet duct. In the lined duct, on assuming a uniform mean flow, the modal decay rates of high-frequency tones are predicted to be typically between 5 and 10 dB, e.g. see Figs. 12 and 13. Inclusion of this small amount of absorption in the numerical simulations has resulted, at high frequencies (high-order EOs), in there being an apparent improvement in the predictions for the lined inlet, compared with the rigid inlet duct. In reality, it is questionable whether, at very high frequencies, this absorption does occur in a lined inlet duct.

5. Conclusions

The FDNS numerical simulation method calculates the nonlinear propagation of the rotor-alone pressure field, generated by a supersonic fan, as it spirals upstream against the oncoming flow in a turbofan inlet duct. Sound attenuation by an acoustic lining is included in the model by the addition of a *linear* absorption term to the nonlinear propagation equation. Therefore, the numerical simulation requires the prediction of modal decay rates in a lined duct.

The FDNS simulation model is a simple engineering scheme, capable of analysing the nonlinear propagation of the rotor-alone pressure field, which is assumed to be the principal source of buzz-saw noise generated by a supersonic ducted fan.

The experimental measurements reveal how buzz-saw noise is affected by an acoustic liner. Most of the characteristic low-frequency buzz-saw tones are absorbed by the lining. The remaining low-frequency tones that are not absorbed by the liner may potentially be a suitable noise source to be controlled by active noise control, see Ref. [21] for preliminary work in this area.

High-frequency buzz-saw tones are unlikely to be absorbed by the type of locally-reacting cavity liners currently used in turbofan engine ducts. At each fan speed, the acoustic liner is most effective in an optimum frequency range. As the fan speed increases, the rotor-alone EO modes become more cut-on, leading to a narrowing in the liner's optimum frequency range, so fewer tones are well absorbed by the lining. Buzz-saw noise will still be detectable radiated from a lined inlet duct, but the characteristic low-pitched noise signature will be altered because the liner will absorb some of the low-frequency tones.

This article presents measurements of the complete buzz-saw noise frequency spectrum, compared with numerical simulations obtained by using the FDNS method that has been developed in earlier work. Results are included for both a rigid and an acoustically-lined inlet duct. As far as the authors are aware, these type of results for a lined inlet duct have not been published before.

Further analysis of the results presented in this article is required to assess the accuracy of the numerical predictions. Two areas of future work are proposed. The first is to examine the effect of a boundary layer on the predicted modal decay rates, and also its possible shielding effect on wall measurements. The second is to examine experimental measurements from the mode detection array, in order to determine whether at low fan speeds there are significant non-rotor-alone noise sources. A subsequent article is planned which will also utilize these new experimental measurements. The aim being to further validate the numerical model, and improve understanding of the generation of buzz-saw noise.

Acknowledgements

The work was funded by the European Community X-noise research projects RESOUND and DUCAT. The support of Mr. P. Kruppa (Technical Monitor for the Commission) is particularly acknowledged.

AM and MJF wish to acknowledge the continuing financial support provided by Rolls–Royce plc.

References

[1] M.G. Philpot, The buzz-saw noise generated by a high duty transonic compressor, ASME Paper No. 70-GT-54, 1970.
[2] D.L. Hawkings, Multiple tone generation by transonic compressors, *Journal of Sound and Vibration* 17 (1971) 241–250.
[3] M. Kurosaka, A note on multiple pure tone noise, *Journal of Sound and Vibration* 19 (1971) 453–462.
[4] M.R. Fink, Shock wave behaviour in transonic compressor noise generation, ASME Paper No. 71-GT-7, 1971.
[5] G.F. Pickett, Prediction of the spectral content of combination tone noise, *Journal of Aircraft* 9 (1972) 658–663.
[6] B.S. Stratford, D.R. Newby, A new look at the generation of buzz-saw noise, AIAA 77-1343, 1977.
[7] A. McAlpine, M.J. Fisher, On the prediction of "buzz-saw" noise in aero-engine inlet ducts, *Journal of Sound and Vibration* 248 (1) (2001) 123–149.
[8] C.L. Morfey, M.J. Fisher, Shock-wave radiation from a supersonic ducted rotor, *The Aeronautical Journal of the Royal Aeronautical Society* 74 (1970) 579–585.
[9] M.J. Fisher, B.J. Tester, P.J.G. Schwaller, Supersonic fan tone noise prediction, AIAA 98-2249, 1998.
[10] A. McAlpine, M.J. Fisher, On the prediction of "buzz-saw" noise in acoustically lined aero-engine inlet ducts, *Journal of Sound and Vibration* 265 (1) (2003) 175–200.
[11] C.L. Bewick, M.J. Adams, P.J.G. Schwaller, X. Lu, Noise and aerodynamic design and test of a low tip speed fan, AIAA 2001-2268, 2001.
[12] W. Eversman, Theoretical models for duct acoustic propagation and radiation, in: H.H. Hubbard (Ed.), *Aeroacoustics of Flight Vehicles*: *Theory and Practice Vol. 2 Noise Control*, NASA RP-1258, 1991, pp. 101–163.
[13] S.W. Rienstra, A classification of duct modes based on surface waves, *Wave Motion* 1107 (2002) 1–17.
[14] R.E. Motsinger, R.E. Kraft, Design and performance of duct acoustic treatment, in: H.H. Hubbard (Ed.), *Aeroacoustics of Flight Vehicles*: *Theory and Practice Vol. 2 Noise Control*, NASA RP-1258, 1991, pp. 165–206.
[15] R. Mittra, S.W. Lee, *Analytical Techniques in the Theory of Guided Waves*, MacMillan Series in Electrical Science, 1971.
[16] D.L. Lansing, W.E. Zorumski, Effects of wall admittance changes on duct transmission and radiation of sound, *Journal of Sound and Vibration* 27 (1) (1973) 85–100.
[17] J.F. Unruh, Finite length tuning for low-frequency lining design, *Journal of Sound and Vibration* 45 (1) (1976) 5–14.
[18] A. Cummings, High frequency ray acoustics models for duct silencers, *Journal of Sound and Vibration* 221 (4) (1999) 681–708.
[19] C.L. Morfey, Sound transmission and generation in ducts with flow, *Journal of Sound and Vibration* 14 (1) (1971) 37–55.
[20] E.R. Rademaker, P. Sijtsma, B.J. Tester, Mode detection with an optimised array in a model turbofan engine intake at varying shaft speeds, AIAA 2001-2181, 2001.
[21] M.J. Wilkinson, P.F. Joseph, A. McAlpine, Active control of buzz-saw tones, *Proceedings of ACTIVE*, Vol. 1, 2002, pp. 357–367.